Retrieval of Atmospheric Parameter Distributions for MIPAS-STR Measurements from the APE-GAIA Flights of 18 October 1999, between Ushuaia, Pôrto Alegre, and Recife

Guillaume PIARD
Imperial College, London

Supervisor:
Dr. Michael Höpfner
Institut für Meteorologie und Klimaforschung
Forschungszentrum Karlsruhe

Abstract

Airborne measurements from the MIPAS-STR[1] instrument, taken during the first two return transfer flights of the APE-GAIA[2] campaign on 18 October 1999, were analysed to derive two-dimensional distributions of atmospheric parameters. Aims of the experiment and measurement methods are introduced, to provide an understanding of the data content used. A description of data calibration (level 1 analysis) and atmospheric parameter derivation (level 2 analysis) is also given. Atmospheric parameter retrievals (the focus of this work) follow, with details of analysis and result discussion for each retrieval. These include temperature, aerosol extinction coefficient, and volume mixing ratios of nitric acid (HNO_3), chlorine nitrate ($ClONO_2$), ozone (O_3), trichlorofluoromethane (CFC-11, CCl_3F), dichlorodifluoromethane (CFC-12, CCl_2F_2), and water vapour (H_2O). Comparison with independent data was made for temperature and HNO_3, thus providing a verification of the results and indications for future improvements.

Kurzfassung

Aus Messungen des MIPAS-STR Geräts, die auf zwei Transferflügen der APE-GAIA Kampagne am 18. Oktober 1999 durchgeführt wurden, wurden zweidimensionale Verteilungen atmosphärischer Parameter abgeleitet. Am Anfang der Arbeit werden die Ziele des Experiments und die Messmethode erklärt. Es schließt sich eine Beschreibung der Kalibrierung (Level-1 Analyse) und der Ableitung atmosphärischer Parameter an. Darauf folgt die ausführliche Darlegung der Level-2 Analyse mit Diskussion der Ergebnisse für folgende atmosphärische Parameter: Temperatur, Aerosol-Extinktionskoeffizient, sowie Volummischungs-verhältnisse von Salpetersäure (HNO_3), Chlornitrat ($ClONO_2$), Ozon (O_3), Trichlorfluormethan (F-11, CCl_3F), Dichlordifluormethan (F-12, CCl_2F_2) und Wasserdampf (H_2O). Für Temperatur und HNO_3 war ein Vergleich mit unabhängigen Daten möglich. Dieser diente zur Verifizierung der Ergebnisse und lieferte Vorschläge zur Verbesserung des Experiments.

[1] Michelson Interferometer for Passive Atmospheric Sounding - STRatospheric aircraft
[2] Airborne Polar Experiment – Geophysica Aircraft In Antarctica

Table of Contents

1 Introduction

The discovery of the so-called ozone hole over Antarctica in 1985 sparked the outbreak of numerous questions concerning the health and evolution of our atmosphere. A continuously growing interest within the international scientific community led to research in the field of stratospheric ozone depletion, which significantly improved our understanding of this phenomenon. Questions remain, however, and ongoing research aims at lifting these uncertainties, in particular to enable a quantitative modelling of the observed processes as well as a good forecasting of the ozonosphere's evolution.

The APE-GAIA campaign was structured in that perspective. Part of the Italian Antarctic Research Program (PNRA[3]), it was aimed at studying the physical and chemical processes responsible for the depletion of the Antarctic stratospheric ozone layer. Using the Russian stratospheric aircraft M55-Geophysica, a combination of in-situ and remote sensing instruments collected atmospheric data from altitudes ranging up to 20 km. Measurement flights took off from Ushuaia in South America and went south into the polar vortex region. Measurements were also performed during the return transfer flights from South America back to Europe, thus providing information about the upper troposphere and lower stratosphere over a wide latitude range.

Among the various instruments present, the Karlsruhe developed MIPAS-STR participated for the first time in a scientific campaign. This Fourier-transform spectrometer was developed with the objective of producing two-dimensional distributions of atmospheric parameters along the flight path, such as for temperature and VMRs[4] of various trace gases. The instrument detects atmospheric mid-infrared emission with a high spectral resolution, and stores the obtained data for later analysis.

This work's focus was to carry out the last part of the data analysis chain (retrievals), for data obtained during the first two return transfer flights of the Geophysica aircraft. These took place on 18 October 1999, between Ushuaia, Pôrto Alegre, and Recife in South America. The retrieved parameters ultimately included temperature, continuum coefficient, and VMRs of HNO_3, $ClONO_2$, O_3, CFC-11, CFC-12, and H_2O. The results will be used by other members of the scientific community in various ways, such as to improve instrument performance, or further the understanding of interactions between the polar and mid-latitude atmosphere.

[3] Programma Nazionale di Ricerche in Antartide

[4] Volume Mixing Ratio

2 The MIPAS-STR Experiment

2.1 The Instrument

2.1.1 Description

The MIPAS-STR instrument was originally developed in view of measuring vertical VMR profiles of trace gases involved in ozone chemistry. It was specially engineered for use onboard of high-flying aircraft, to carry out measurements along the flight path [Piesch and others 1996]. This new use of the Michelson Interferometer is an expansion and improvement of two already existing experiments, namely MIPAS-FT[5] and MIPAS-B2[6]. The former gathered atmospheric data along the plane's flight path, whereas the latter sounds different atmospheric layers from a stratospheric balloon. MIPAS-STR is capable of both, which enables it to produce two dimensional distributions of atmospheric measurements. Figure 2.1.1 shows how obtaining information from different atmospheric layers is possible. With a scanning technique known as limb sounding, the instrument changes its observation angle in the atmosphere using a rotational mirror. The altitude of observation corresponding to a certain limb angle is geometrically determined by the tangent height of the LOS[7]. The optical path passes predominantly through the atmospheric layer corresponding to the associated tangent point, hence mostly seeing information from this specific layer.

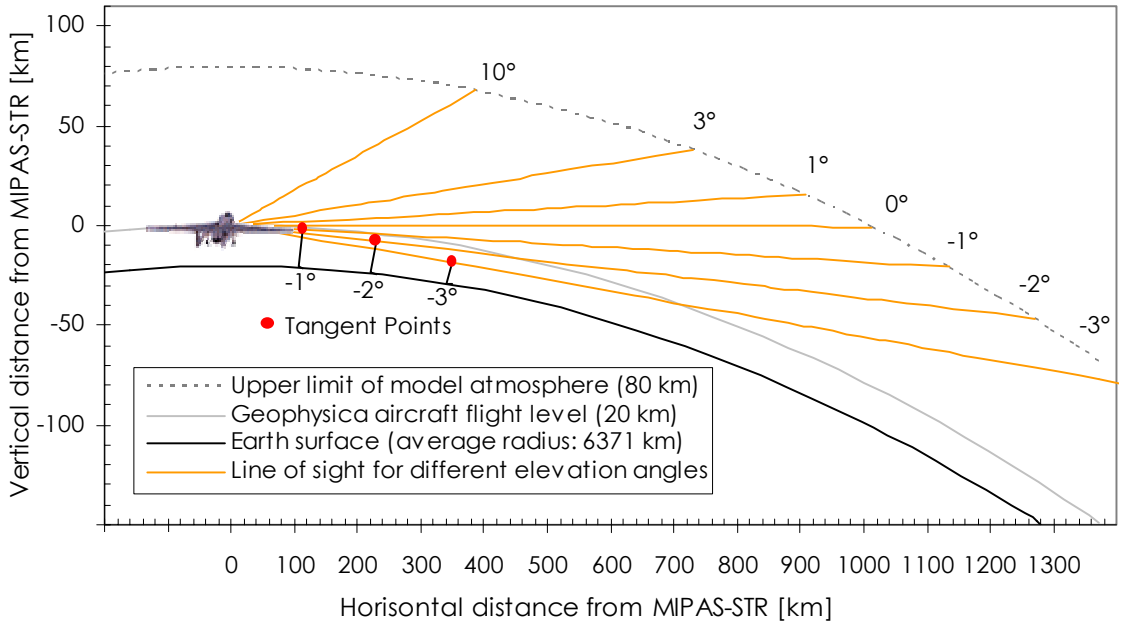

Figure 2.1.1: Observation of different atmospheric layers using the limb sounding technique

[5] MIPAS - Flugzeug Transall

[6] MIPAS for Balloon

[7] Line Of Sight: optical path of the instrument through the atmosphere

The physical principle behind the instrument is the detection of rovibrational transitions of gas molecules. Many atmospheric trace gases have characteristic spectral signatures of such transitions in the mid-infrared range. Using a high-resolution interferometer built following the Double Pendulum Principle [Fischer 1992], MIPAS-STR measures atmospheric spectral emission, storing the results in the form of interferograms, which are later Fourier-transformed into spectral radiance data. This interferometer is, therefore, an FTIR-Spectrometer[8], which has the advantage of measuring radiance for a broad spectral range simultaneously. The strength of MIPAS-STR lies in the broadness of this spectral range from 770 – 1940 cm^{-1}, distributed in four channels, which can identify the whole NO_y gas family, part of the Cl_y family, and a number of other trace gases such as $ClONO_2$, HNO_3, N_2O, NO, NO_2, etc.

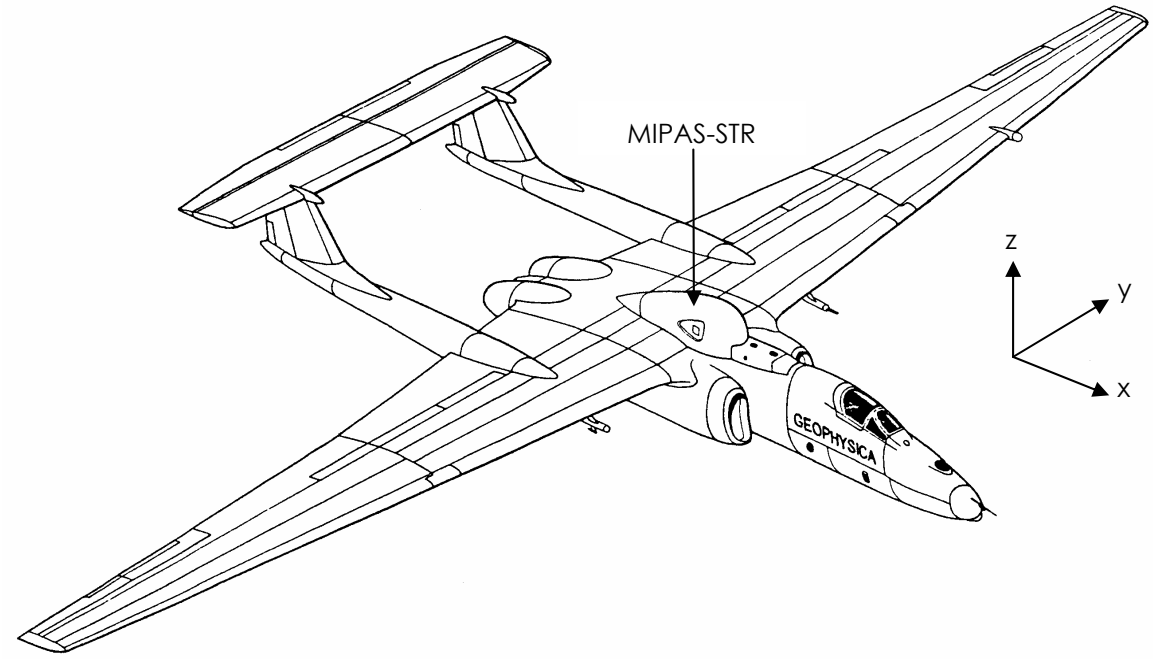

Figure 2.1.2: Lateral view of the M55-Geophysica with the MPIAS-STR hood in place

MIPAS-STR's main component is the optics module, which sits on top of the Geophysica underneath a specially built hood. Figure 2.1.2 shows the aircraft with the hood in place. The instrument observation window situated on the right side of the aircraft is visible. This optics module, which can be seen in Figure 2.1.3 on the next page, is built into a structural frame designed to limit the impact of aircraft vibrations. Once the radiation reaches the rotational mirror, it passes through a system of mirrors and lenses which filter most of any unwanted scattered light, before it goes through the interferometer and the detector unit. Ultimately, the detector sees a cone shaped portion of the atmosphere with a vertical angle component of 0.48° (for the full cone). This corresponds to a vertical FOV[9] resolution of about 2.5 km for a 10 km tangent height and a 17 km flight level.

[8] Fourier Transform InfraRed - Spectrometer

[9] Field Of View

In an attempt to minimise thermal radiation from the instrument itself, which would falsify the measurements, the whole system is isolated and cooled with dry-ice. The detector unit is directly cooled with liquid helium. Background heat still remains, however, and its value can drift with time. This requires it to be measured in order to secure an absolute calibration of the experimental data. A hot and a cold blackbody with known temperatures are used to this effect.

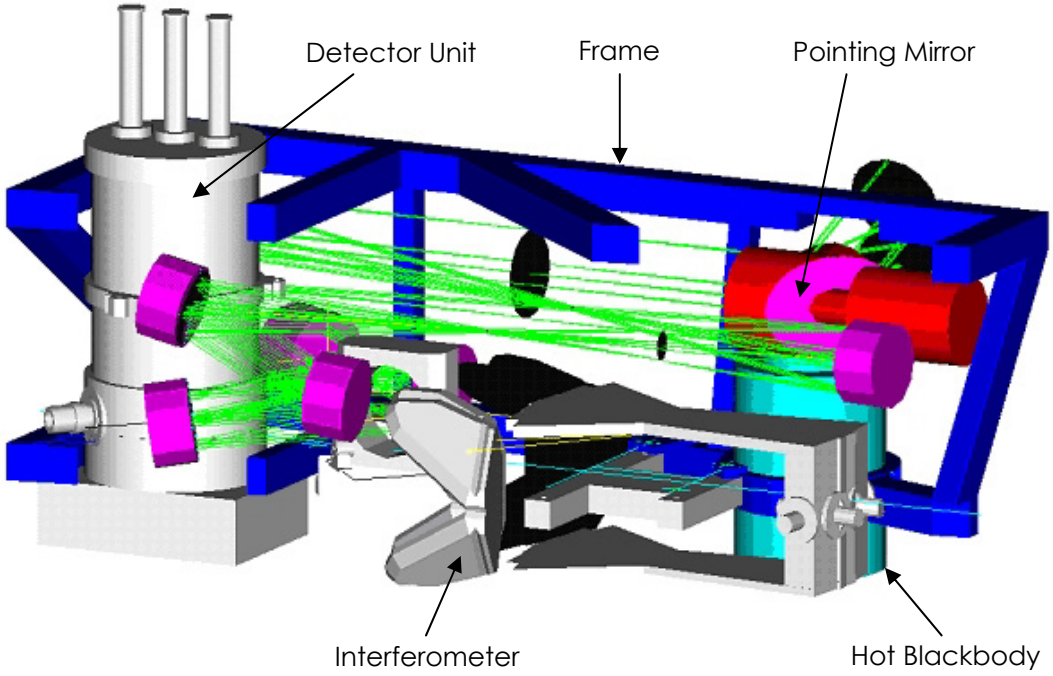

Figure 2.1.3: Three-dimensional perspective of the MIPAS-STR optics module

All the electronics necessary for instrument operation are housed together in a processing unit. It includes a central computer for global system management, LOSE[10] for pointing mirror control, and IFME[11] for double pendulum control and data intake. A linkup with the processing unit is possible through a base station while the plane is in the hangar. This enables testing procedures, reading out of in-flight measurement data, as well as complete system parameter configuration [Piesch and others 1996].

[10] Line Of Sight Electronics
[11] InterFeroMetric Electronics

2.1.2 Calibration for 18 October 1999

Table 2.1.1 contains some of the main parameter values effective for the two flights of 18 October 1999. Data used for this work came from channel 1, with a spectral resolution of 0.043 cm^{-1} at FWHM[12], and a wavenumber range of 770 – 970 cm^{-1}.

Interferometer

maximum optical path difference	14.1 cm
path alteration speed	3.1 $cm.s^{-1}$
etendue	$2.6*10^{-3}$ cm^2 sr
spectral resolution	0.043 cm^{-1}
optical cross-section	50 mm

Detector

type	SiAs
FOV	0.48°
signal frequencies	2.3 – 5.8 kHz

NESR[13]

channel 1:	770 – 970 cm^{-1}	(10.0 – 13.0 µm)	30 nW/(cm^2 sr cm^{-1})
channel 2:	1200 – 1370 cm^{-1}	(7.3 – 8.3 µm)	45 nW/(cm^2 sr cm^{-1})
channel 3:	1585 – 1645 cm^{-1}	(6.1 – 6.3 µm)	20 nW/(cm^2 sr cm^{-1})
channel 4:	1845 – 1940 cm^{-1}	(5.2 – 5.4 µm)	6 nW/(cm^2 sr cm^{-1})

Blackbodies

cold (1)	emission coefficient	0.997
	temperature	205 K
hot (2)	emission coefficient	0.980
	temperature	240 K

Table 2.1.1: MIPAS-STR parameters overview for 18 October 1999

[12] Full Width at Half Maximum

[13] Noise Equivalent Spectral Radiance

2.2 Obtaining the Data

2.2.1 Measurement Strategy

The measurement procedure used during the APE-GAIA campaign – and hence also for the return transfer flights from Ushuaia back to Europe – was a combination of atmospheric limb scans below the aircraft, and upward sounding above the flight level. Geometries below the aircraft contain more information about altitude distribution, since the main contribution of radiance comes from the tangent point area associated with a know tangent height (cf. Figure 2.1.1). Sounding above the aircraft contains little altitude information due to nonexistent tangents, but can nevertheless still give an idea of the vertical profile shapes at those higher altitudes [Höpfner, Blom, Echle, and others 2001].

Figure 2.2.1 on the next page shows a sample of the measurement sequence which was used. Atmospheric measurements were taken for mirror angles between -3.1° and +3.0°. Following a report on retrieval simulations for the MIPAS-STR instrument [Höpfner, Blom, Echle, and others 2001], which determined that a FOV overlap increased vertical profile resolution for lower geometries, the measurement grid was set to 0.5 FOV for lower geometries, and 1.0 FOV for higher ones. This led to a total of 14 atmospheric scans. Between each atmospheric sequence, deep space measurements at +10°, as well as hot and cold blackbody measurements at ±90° were taken for data calibration [Höpfner, Blom, v. Clarmann, and others 2001].

The time needed for the creation of each interferogram is calculated with the formula (2 x optical path / path alteration speed) + 1 second for interferometer direction switch. The result here was about 10 seconds, leading to a horizontal resolution for each 14 scan profile of about 30 kilometres along the flight path.

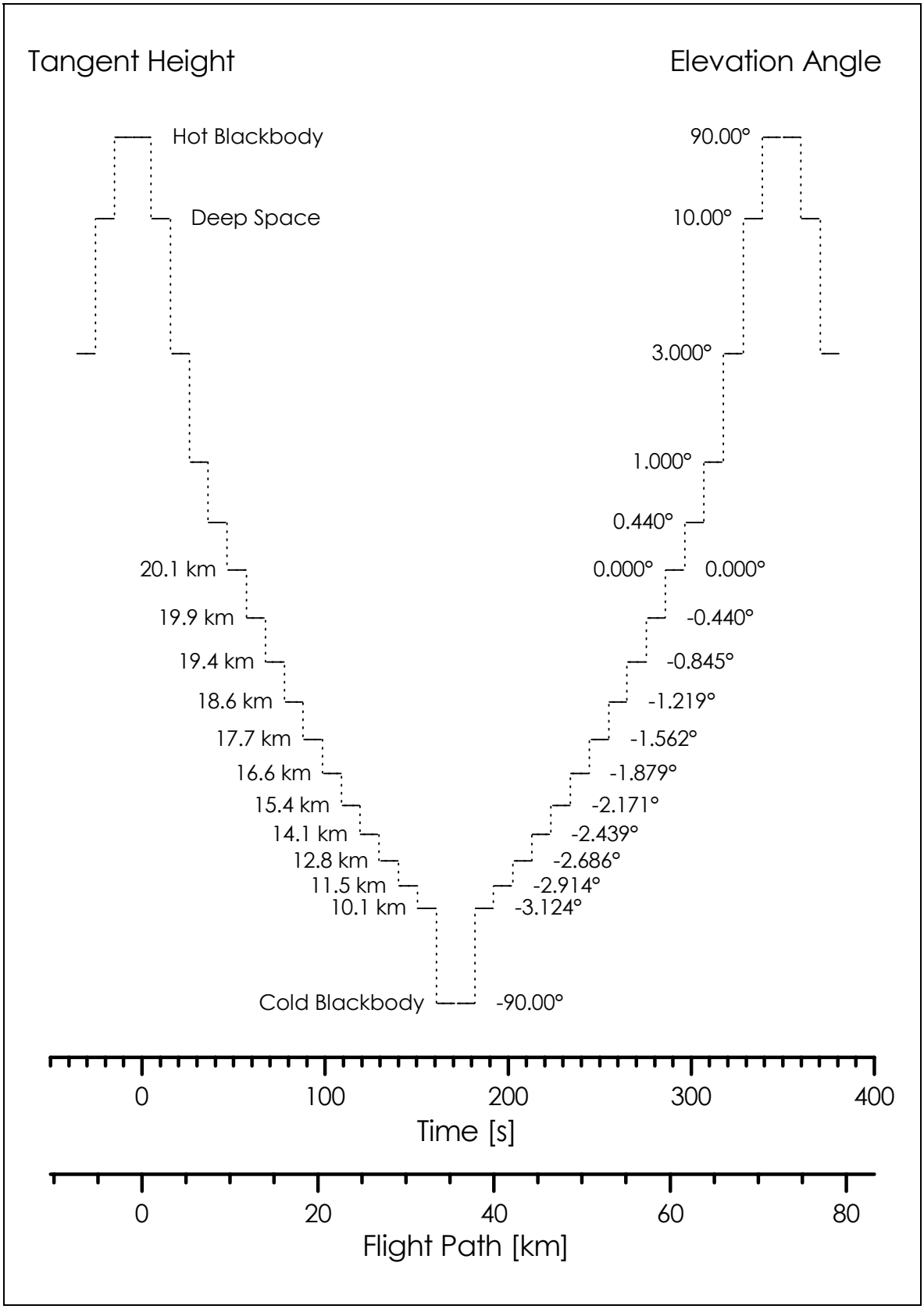

Figure 2.2.1: LOS scan sequence of MIPAS-STR for the flights of 18 October 1999

2.2.2 Flight Information for 18 October 1999

The flights analysed were the first two of a series of four back to Europe. The M55-Geophysica took off from Ushuaia in Terra del Fuego, Argentina (54.85° S, 68.31° W) at 09:24 UTC[14] with a north-northeast heading. In Pôrto Alegre, Brazil (30.02° S, 51.13° W) it made a fuel stop at 14:20 UTC. The second flight continued at 17:30 UTC along the South American coast to Recife, Brazil (08.06° S, 34.53° W), situated on the eastern tip of the continent, with a landing at 22:15 UTC. No significant problems were reported.

Figure 2.2.2 shows altitude profile sections of the two flights. GPS[15] altitude had to be corrected due to SA[16], which could have led to errors of the order of 100 meters. First, a pressure altitude was calculated by correlating onboard pressure and temperature measurements with ECMWF[17] P-T profiles. This altitude profile is correct in shape, but can contain an offset due to errors in ECMWF analysis. This offset was corrected by adding the average difference between the two altitudes, which gives the corrected altitude. The data used for retrieval calculations was divided into 6 regions, where the aircraft had a stable flight level.

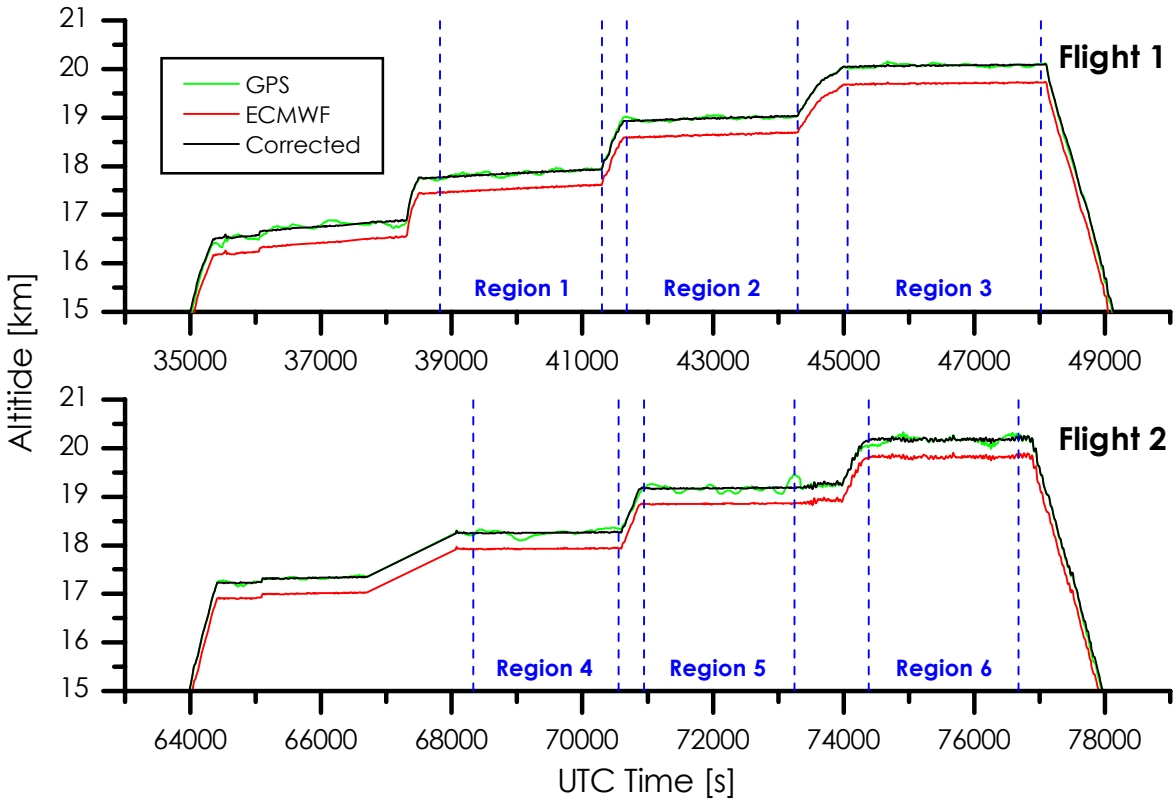

Figure 2.2.2: Flight altitude profiles in regions where measurements were made

[14] coordinated universal time, formerly GMT
[15] Global Positioning System
[16] Selective Availability, service quality restriction used by the US military, no longer active
[17] European Centre for Medium-range Weather Forecasts

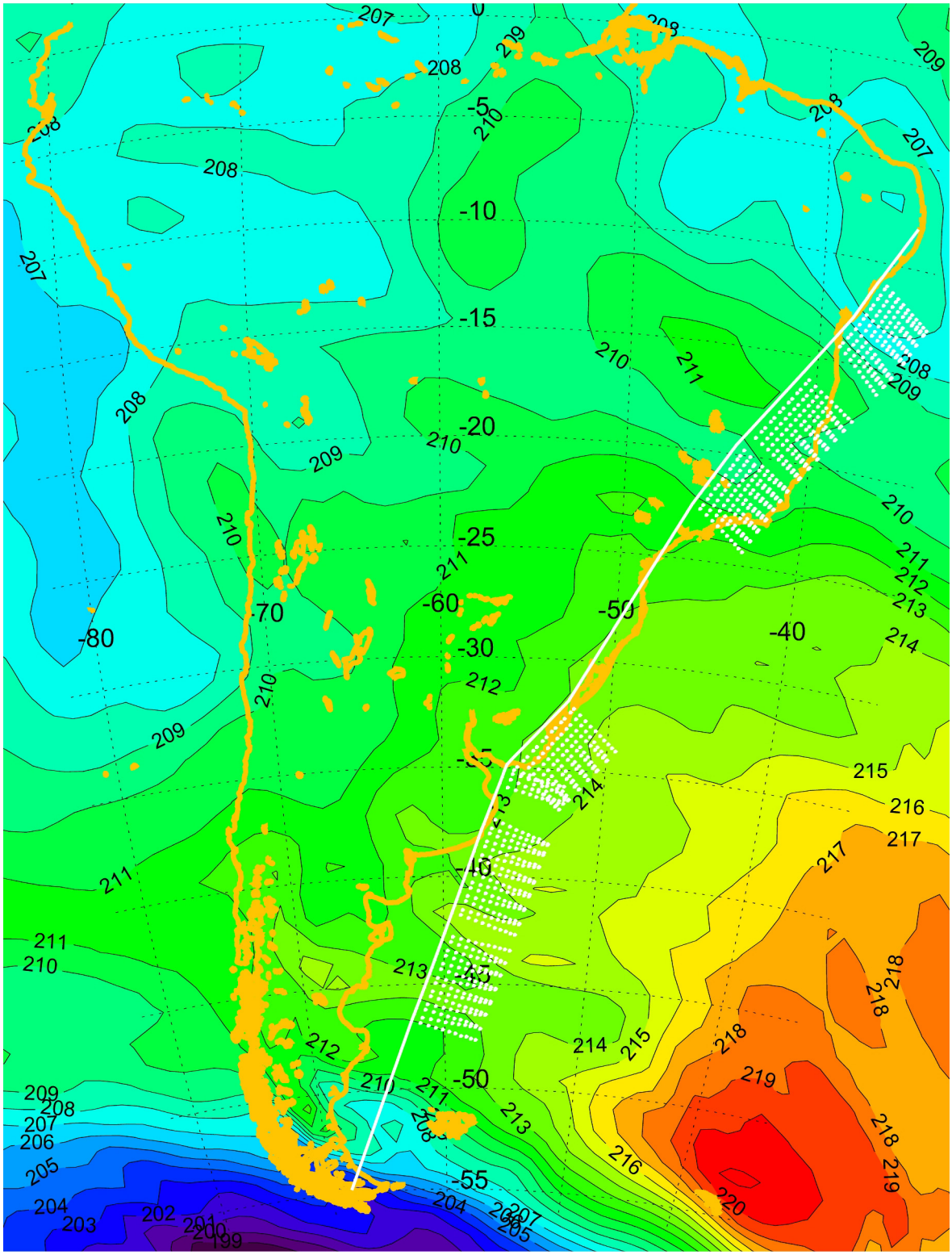

Figure 2.2.3: Geophysica flight path for 18-10-1999 along the South American coast (line) with measurement tangent points (dots), and temperature map [K] for flight level at 70 hPa

Figure 2.2.3 shows the trajectory taken by the Geophysica with measurement tangent points along the right side of the flight path. The temperature map has been set to a 70 hPa level, which corresponds to the average aircraft pressure altitude during measurements.

2.3 Level 1 Data Processing: Preparing the Data for Atmospheric Parameter Retrieval Calculations

Post-flight level 1 data processing consists in preparing the data in a form usable by computer programs to perform atmospheric parameter retrievals, and proceeds in several steps. First, a phase correction was used to Fourier-transform the interferograms into spectra [Höpfner, Blom, v. Clarmann, and others 2001]. Figure 2.3.1 shows the real and imaginary parts of a single example spectrum. The spectral information could not be used as is, as it first required calibration. Blackbody and deep space measurements were used to this effect [Höpfner, Blom, v. Clarmann, and others 2001].

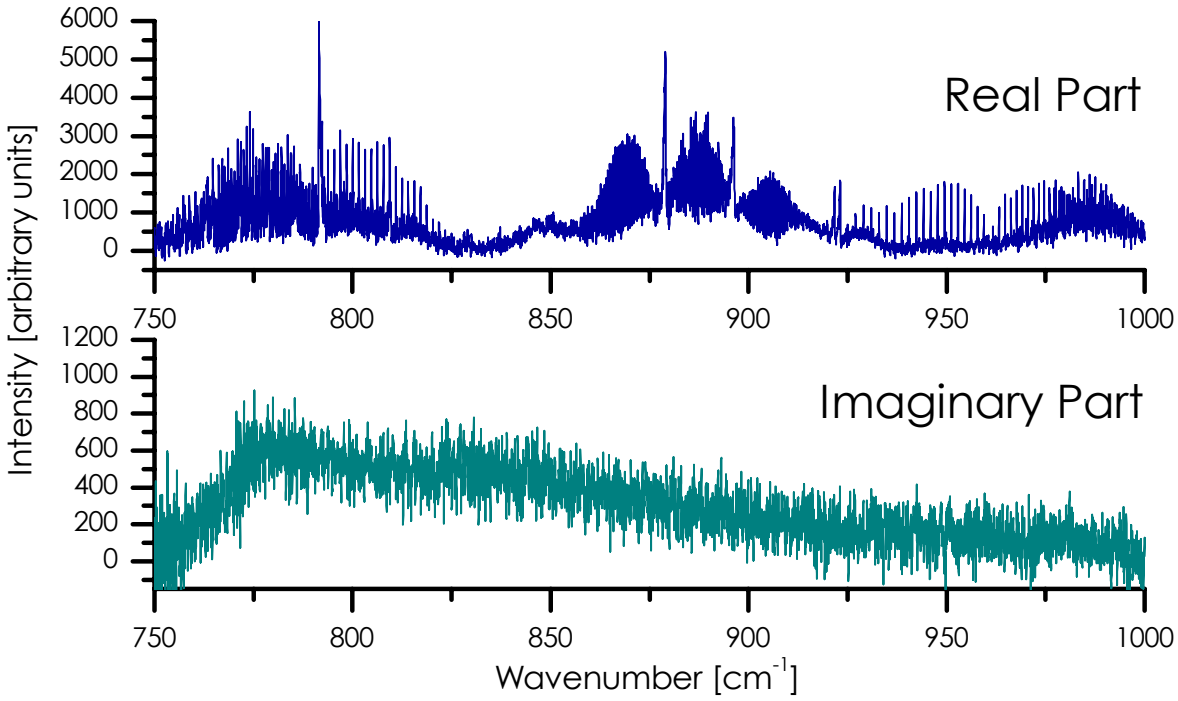

Figure 2.3.1: Real and imaginary parts of a single atmospheric spectrum after phase correction (tangent altitude = 15 km)

Other calculations were made to determine errors arising through corrections. Deep space calibration measurements induced an error of up to 1% in the detector gain calibration function, due to imperfect deep space spectra simulations. An additional error in the gain function, also taken into account, was probably induced by aircraft vibrations [Höpfner, Blom, v. Clarmann, and others 2001].

The last step involved manually eliminating corrupt or unusable data. Temporary malfunction of instrumentation is an example cause of corrupt data. Measurements where the aircraft did not have a stable flight level were not usable due to inconsistencies in measurement tangent heights. Clouds, due to their grey-body nature, distort atmospheric emission and lead to poor spectral information, which also had to be eliminated for the concerned geometries.

2.4 Level 2 Data Processing: Retrieval of Atmospheric Parameter Distributions

The focus of this work was to complete level 2 analysis calculations for temperature and the gases mentioned in the introduction, with the use of the two computer algorithms KOPRA[18] and KOPRAFIT[19].

2.4.1 Forward Model Calculations Using KOPRA

The forward model algorithm KOPRA is a fast line-by-line code used to calculate radiative transfer, especially developed for the analysis of data measured by high-resolution interferometers. It is capable of simulating numerous physical aspects of atmospheric radiative transfer such as non-spherical ray tracing, line-mixing, NLTE[20], and aerosols. It supports all observational geometries, and so can be used to analyse data originating from other instruments than the MIPAS-STR. Apart from atmospheric properties, KOPRA can also simulate a number of instrumental effects including finite FOV and ILS[21]. Parallel to the forward calculation of radiative transfer, the algorithm analytically determines the derivatives of the spectrum with respect to many atmospheric and instrumental parameters [Stiller and others 1998]; [Stiller (Editor) and others 2000].

These calculations are broken down into several smaller sub-calculations, the first of which is ray tracing. Consisting in calculating the precise trajectory of the LOS, it uses as input the coordinates of the aircraft (latitude, longitude, altitude, heading), as well as the elevation angle of the instrument, to determine the spatial coordinates of the measurement tangent points, taking the atmospheric refractive index gradient into account (cf. Figure 2.2.3).

Next in line is the simulation of radiative transfer for the concerned atmospheric layers along the LOS. An estimation of the atmospheric state is needed here. This is calculated outside of KOPRA, using ECMWF data for pressure and temperature, through an interpolation with measurement tangent point positions. Due to the nature of the measurements, the distance between tangent points can be up to 250 km (cf. Figure 2.1.1), and so interpolating the atmospheric data gives better results in following calculations than using simple profiles at aircraft position.

The last segment of code is responsible for the instrumental effects simulation, such as FOV properties, or ILS. KOPRA offers good control over all simulation parameters through an extensive calculation configuration input file.

[18] Karlsruhe Optimised and Precise Radiative transfer Algorithm
[19] Algorithm extension from KOPRA
[20] Non-Local Thermodynamic Equilibrium
[21] Instrumental Line Shape

2.4.2 Inversion Calculations Using KOPRAFIT

The inversion model KOPRAFIT is used to retrieve atmospheric parameters. This is done by fitting the simulated spectral information from KOPRA to the measured spectra, through one of several different iterative processes available. This retrieval algorithm is capable of fitting all scan geometries from a complete scan sequence (cf. Figure 2.2.1) in many spectral intervals simultaneously [Höpfner, v. Clarmann, and others 1998]

Retrieval of an atmospheric parameter began with the selection of spectral intervals containing information about the chosen parameter (CO_2 lines for temperature, specific gas lines for gas VMRs). These spectral intervals, called microwindows, allow KOPRA and KOPRAFIT to run using only the required spectral data, thus greatly decreasing calculation times and minimising interference from unwanted spectral signatures. The calibrated measured spectra from these spectral intervals were extracted for each scan geometry, and written out into so-called spectral measurement vectors. Corresponding simulated spectra from the forward model calculations were written out into spectral simulation vectors.

Once theses vectors were constructed, they were fed into the inversion calculation for which several retrieval methods are possible. Data from 18 October 1999 was analysed using the Tikhonov-Philips regularisation method [Tikhonov 1963]; [Phillips 1962] in the following form:

$$x_{i+1} = x_i + \left(\mathbf{K_i^T S_y^{-1} K_i} + \gamma \mathbf{L^T L}\right)^{-1} \left[\mathbf{K_i^T S_y^{-1}} \left(y - f(x)_i\right) + \gamma \mathbf{L^T L}\left(x_a - x_i\right)\right] \qquad \textbf{Equation 1}$$

where i = iteration index
x = vector with the unknowns
x_a = initial guess values
y = measurement vector
$\mathbf{S}_y$ = covariant matrix of y
f = forward model
$\mathbf{K}$ = spectral derivatives matrix
γ = regularisation parameter
$\mathbf{L}$ = first derivative regularisation operator

The solution to Equation 1 is constraint to the shape of an initial guess used as a reference profile, and is dependent on γ and the information content of the measurement vector. Regularisation was necessary due to a measurement grid of 0.5 FOV for lower tangent heights (smaller than the resolution of the instrument), which induces an unbalance in unknowns of the equation. Each retrieved atmospheric parameter has a regularisation parameter γ, which was determined following two main criteria: Its value had to be big enough to avoid instabilities in the profile shape, but be kept as small as possible to minimise the RMS[22] between the measured and simulated spectrum [Höpfner, Blom, Echle, and others 2001].

[22] Root Mean Square

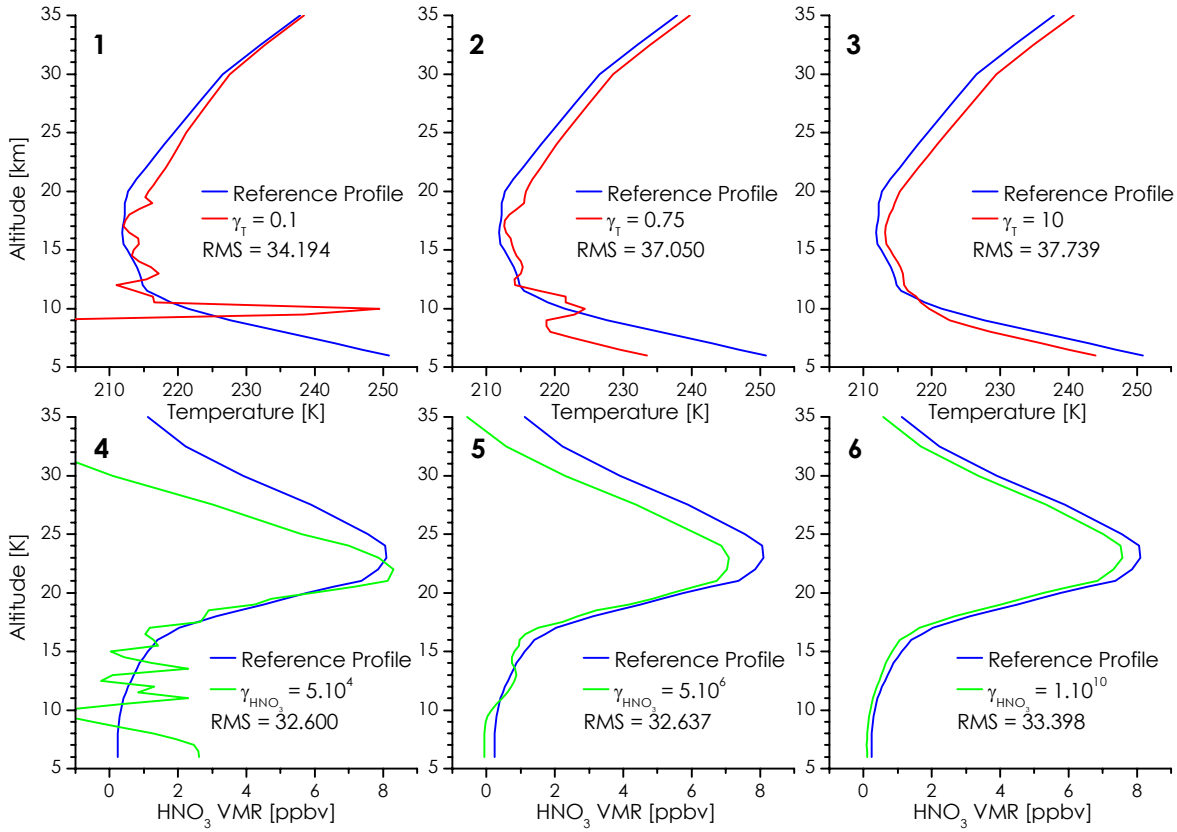

Figure 2.4.1: Example retrieval calculations for temperature and HNO_3 VMR using the Tikhonov-Phillips regularisation method, with different regularisation strengths

Figure 2.4.1 illustrates the effect of different regularisation strengths on parameter retrievals. The first row of graphs contains vertical profiles of temperature, whereas the lower row shows vertical profiles of HNO_3 VMR. In both, the blue curve represents the initial guess (reference profile) of the inversion calculation, and the other curve represents the result. The regularisation parameter γ increases from left to right.

With a too weak regularisation, the result has a tendency to oscillate around the reference profile, as can be seen in graphs 1 and 4. This is a clear sign that γ_T and γ_{HNO3} need to be bigger. When on the contrary the regularisation is too big, information about the measurement is no longer taken into account sufficiently. This leads to a result which quite strictly follows the initial guess, without having enough freedom to attempt a fit to the measurement. As a consequence, the RMS between the measured and simulated spectra increases. This is the case for graphs 3 and 6.

Graphs 2 and 5 show a compromise between these two extremes. Strong instabilities in the profile shape are eliminated, but still leave enough freedom to the calculation to bring out information contained in the measurement spectra. This situation was determined through trial and error with different γ values. It was important to make educated guesses rather than trying random values, as each retrieval calculation could take up to 30 minutes or more for the complete set of flight data, thus quickly leading to very time consuming work.

2.4.3 Error Assesment

Errors in the measured spectra have various origins. One of the most important errors arises through data calibration, and is composed of two parts (cf. section 2.3). The first is a systematic error linked to the averaging of the instrument gain function, and is estimated to be about 1%. The second, of statistical nature, is primarily linked to aircraft vibration and is estimated to be about 5%. Other errors are connected to the use of HITRAN[23] spectral line data for the radiative transfer calculation in the forward model [v. Clarmann and others 1998] (cf. section 2.4.1). The error here is estimated to be about 3-5%. Effects such as NLTE, uncertainties in the LOS of the instrument, or horizontal atmospheric inhomogeneity can cause further statistical errors as well, which are difficult to estimate, but which were considered insignificant in order of magnitude for the measurement geometries used.

It is to date extremely difficult to estimate a precise total error for the retrievals since many factors are not well known or understood. This is still in development phase within the retrieval algorithm. It is however possible to calculate the error linked to instrumental noise (NESR). This spectral noise in the measurement is transferred to an error in parameter profiles [Tikhonov 1963]; [Phillips 1962] through the following relation:

$$\mathbf{S}_x = \left(\mathbf{K}^T\mathbf{S}_y^{-1}\mathbf{K} + \gamma\mathbf{L}^T\mathbf{L}\right)^{-1}\mathbf{K}^T\mathbf{S}_y^{-1}\mathbf{K}\left(\mathbf{K}^T\mathbf{S}_y^{-1}\mathbf{K} + \gamma\mathbf{L}^T\mathbf{L}\right)^{-1} \qquad \textbf{Equation 2}$$

where x = vector with the unknowns
y = measurement vector
$\mathbf{S}_x$ = covariant matrix of x
$\mathbf{S}_y$ = covariant matrix of y
$\mathbf{K}$ = spectral derivatives matrix
γ = regularisation parameter
$\mathbf{L}$ = first derivative regularisation operator

This NESR error and its vertical span in the retrievals are both dependent on the DF[24] of the profiles. DF is a measure of how much liberty the profile has to follow measurement information and not the reference profile. It is itself dependent on regularisation parameter strength, as well as instrument FOV and observation angle [Höpfner 2002]. The error is calculated by the inversion model KOPRAFIT and examples have been plotted for the various atmospheric parameter retrievals (cf. section 3).

[23] HIgh-resolution TRANsmission molecular absorption database
[24] Degrees of Freedom

3 Retrievals

3.1 Temperature

3.1.1 Calculation Procedures

Common procedure for the retrieval of temperature is the use of CO_2 spectral lines, on grounds that the VMR profile is very well known for this gas. Furthermore, atmospheric emission in the used wavelength range is primarily dependent on temperature, which helps for this retrieval procedure. 4 spectral microwindows were chosen within channel 1 (cf. Table 2.1.1), for wavenumbers where little or no influence from other gas lines was noticeable. This is important for good retrievals, and also simplifies the retrieval procedure; in the presence of different gases, these would have had to be included in the retrieval with further regularisation parameters (γ) to determine, leading to longer calculation times and potentially poorer result quality. Spectral shift and offset were also fitted in the retrieval calculation, although not regularised. All other parameters for the forward and inversion calculations were left as standard. A summary of the final retrieval parameters used is given in Table 3.1.1.

Microwindows [cm^{-1}]	
1	941.5 – 945.0
2	950.5 – 952.0
3	952.0 – 953.5
4	954.0 – 957.0

Fitted Parameters	
temperature	γ_{Temp} = 0.75 (typical DF = 6.5 – 7.5)
shift	(no regularisation)
offset	(no regularisation)

Other Settings	
regularisation method	Tikhonov-Phillips with constraint to a mid-latitude reference profile shape
regularisation iterations	5
reference profiles	ECMWF field (resolution: 1.25°x1.25°) interpolated to tangent points

Table 3.1.1: Retrieval parameters for temperature

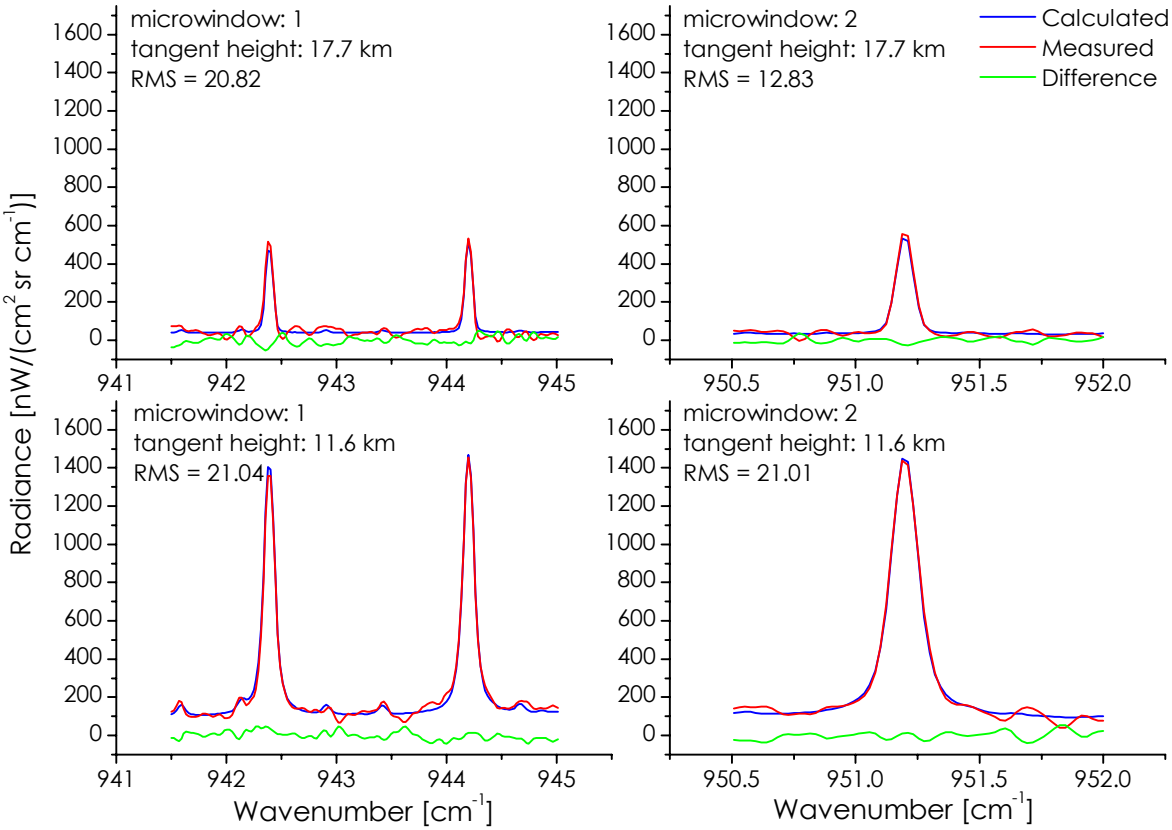

Figure 3.1.1: Sample spectral data for temperature retrieval from microwindows 1 and 2, and geometry tangent heights of 11.6 km and 17.7 km

Figure 3.1.1 shows samples of spectral data used to retrieve temperature. Spectral lines seen here are from CO_2, with measured values in red and calculated values in blue. The RMS between the two spectra is calculated using the difference, also plotted here in green. Both microwindows in this example clearly show a decrease in radiance with altitude. Since gas VMR is constant within the tropopause, and hence between these two tangent heights, these graphs illustrate the dependence of radiance with pressure and temperature.

During the retrieval calculations for temperature, it was noticed that regions 4 and 5 contained poor information for lower tangent heights due to clouds. Some of the bad data had not been eliminated during phase 1 calculations. Clouds have a tendency of absorbing atmospheric emission and reemitting it over a broad spectral range, thus diminishing spectral line intensities and creating an offset in the spectrum. With the chosen calculation settings, KOPRAFIT eliminated the offset, but was unable to account for diminished line intensities. These were simply interpreted as a reduction in temperature, and led to false profiles. Therefore, the concerned geometries had to be eliminated from the calculations.

3.1.2 Results and Observations

Figure 3.1.2 shows a retrieved temperature profile from region 6 corresponding to one complete scan sequence from the MIPAS-STR instrument.

The used γ_{Temp} value of 0.75 was noticeably larger than other values (0.1) used in retrievals from previous flights. This is probably due to stronger noise in the spectra for the flights of 18 October 1999. Statistical errors due to NESR are represented by the error bars, and are of the order of 0.5 K. It should be noted that although these error bars have been drawn every 500 meters, the real vertical error span is dependent on the DF (cf. section 2.4.3). Less degrees means a larger error span.

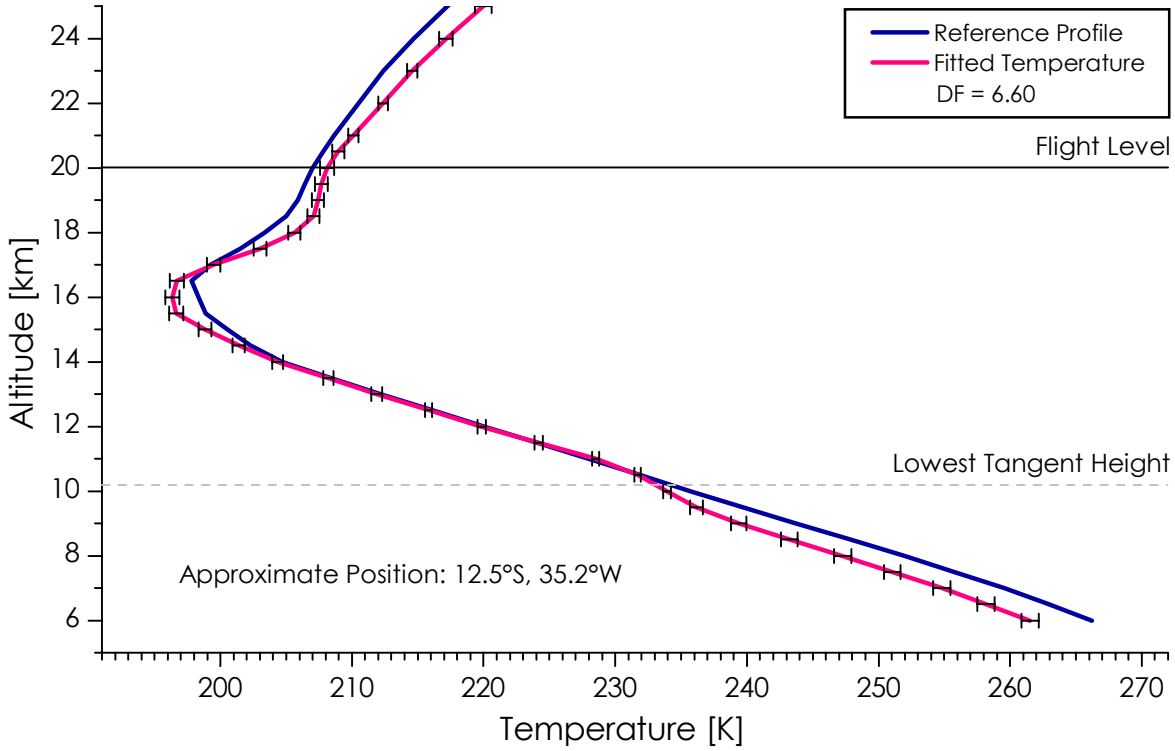

Figure 3.1.2: Retrieved temperature profile from region 6 with NESR error and initial guess

Two-dimensional temperature distributions for the flights of 18 October 1999 are shown on the next page in Figure 3.1.3 and Figure 3.1.4. The top plot shows the interpolated ECMWF data which was used for the reference profiles. The retrieved temperature distribution is underneath. Both contours were obtained through linear interpolation of the individual profiles. The uppermost crosses in each plot indicate flight altitude during measurements, whereas the lower crosses in the fitted temperature indicate the lowest tangent heights used for the calculations. It is important to note here that regions 4 and 5 contain very little truthful information, due to few available observational geometries. All information under the lowest tangent heights should be ignored in these regions, for it is basically a reproduction of initial guess values.

Unlike previous flights of the APE-GAIA campaign, the two from 18 October 1999 had a relatively constant north-northeast heading, which allowed for plots against latitude instead of time. This gives a nice cross-section cut of the atmosphere and shows the change of atmospheric conditions between the polar and equatorial regions. Visible here for example is the 4 km rise of the tropopause as the equator is approached. At 56°S it is at 12 km, where as at 12°S it is at 16 km. This change in air temperature is in fact also visible in Figure 2.2.3.

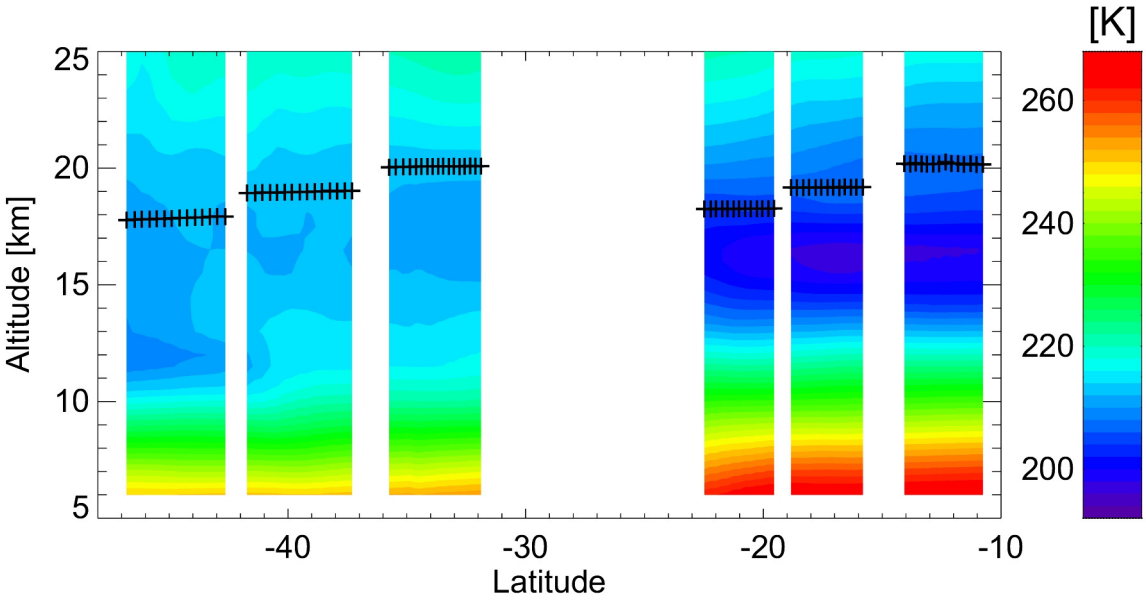

Figure 3.1.3: Two-dimensional distribution of initial guess (ECMWF data) for temperature

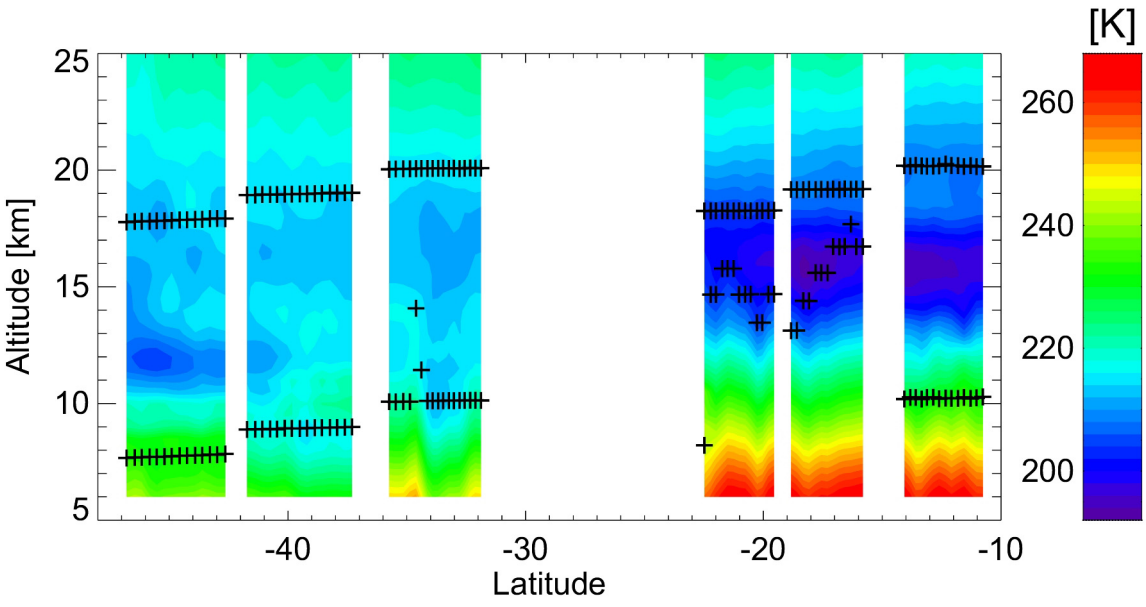

Figure 3.1.4: Two-dimensional distribution of retrieved temperature

3.1.3 Comparison with ECMWF and In-Situ Data

It is quite difficult to estimate total error for these retrieval calculations since the different error factors are not all precisely known or understood (cf. section 2.4.3). However, it was possible to compare the results with other data, to get an idea of their quality. Comparisons were possible at flight level with ECMWF data, as well as in-situ measurements which were taken during the flights. For other altitudes between 16 and 12 km, comparisons with ECMWF data were made. MIPAS-STR data from regions 4 and 5 was not considered below 16 km. These comparisons are visible in Figure 3.1.5 on the next page.

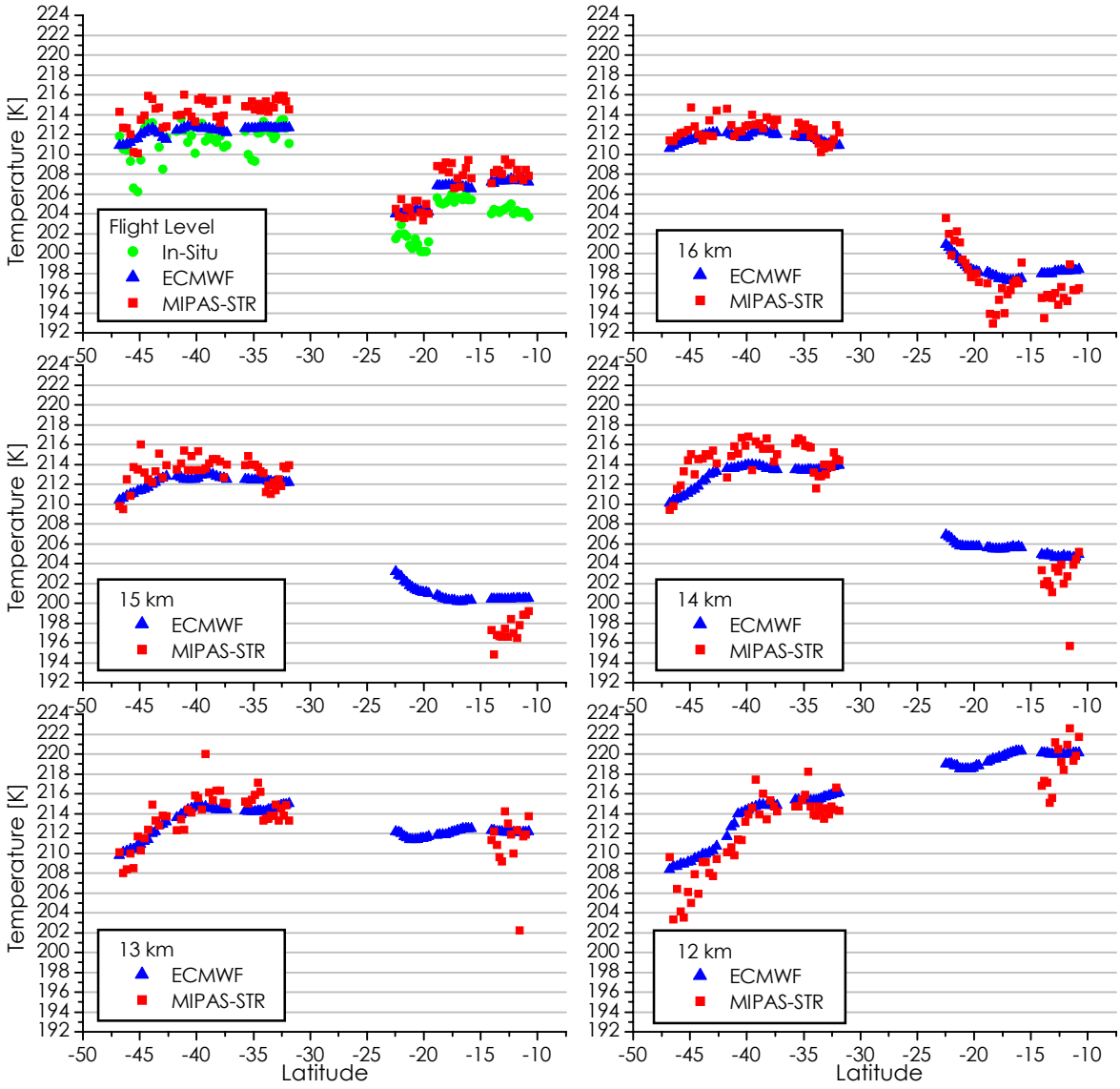

Figure 3.1.5: Temperature result comparisons with in-situ and ECMWF temperature data

At flight level, the MIPAS-STR measurements follow the evolution of in-situ measurements very well. Even in regions 1 and 2, where the temperature is not stable, the two sets of data follow a similar pattern. However, there is a constant offset between the values, with in-situ measurements being on average 3.1 K colder. This had also been noticed for retrievals from other flights during the APE-GAIA campaign. This could be linked to a known existence of errors in the in-situ temperature data, or perhaps due to scattering from dust particles on the pointing mirror (cf. Figure 2.1.3) [Keim 2002]. Nevertheless, this comparison is encouraging, as it shows that MIPAS-STR is capable of detecting small temperature differences.

For 16, 15 and 14 km, a similar offset between ECMWF and MIPAS-STR data is seen. MIPAS-STR is on average 1.05 K hotter for the first flight and 2.56 K colder for the second (ignoring regions 4 and 5). The most likely explanation is an imperfect analysis from the ECMWF. The second flight offset is not surprising, as ECMWF data is known to be too warm in the tropical tropopause. At 13 and 12 km, the data fits generally quite well, apart from one or two isolated measurements.

3.2 Continuum

3.2.1 Calculation Procedures

Continuum[25] is not a parameter which the MIPAS-STR was normally made to measure. Nevertheless, given the fact that significant clouds were present in regions 4 and 5, the opportunity was taken to see if it was at all possible to detect them in a continuum retrieval calculation, and if yes, how well this could be done.

This calculation was based on the same settings as for temperature retrieval, with a few changes. All limb scan geometries which had been previously eliminated from calculations due to clouds were this time included. In the forward model, continuum derivatives were calculated instead of offset. Correspondingly, continuum was fitted instead of offset in the retrieval model. Four regularisation parameters were used, since each microwindow required its own, but these were not varied independently. A summary of the final retrieval parameters used is given in Table 3.2.1.

Microwindows [cm^{-1}]	
1	941.5 – 945.0
2	950.5 – 952.0
3	952.0 – 953.5
4	954.0 – 957.0

Fitted Parameters	
continuum mw 1	γ_{con1} = 1.25 x 10^8 (typical DF = 10.1 – 10.5)
continuum mw 2	γ_{con2} = 1.25 x 10^8 (typical DF = 9.3 – 10.0)
continuum mw 3	γ_{con3} = 1.25 x 10^8 (typical DF = 9.3 – 10.0)
continuum mw 4	γ_{con4} = 1.25 x 10^8 (typical DF = 10.0 – 10.7)
temperature	γ_{Temp} = 0.75 (typical DF = 6.6 – 7.5)
shift	(no regularisation)

Other Settings	
regularisation method	Tikhonov-Phillips with constraint to a mid-latitude reference profile shape
regularisation iterations	8

Table 3.2.1: Retrieval parameters for continuum

The Continuum retrieval led to some difficulties, mainly due to continuum simulation problems. The spectral data showed that there were actually two cloud layers in some regions, since the spectral measurement vectors contained two continuum peaks. This is visible in the left graph of Figure 3.2.1, where the two

[25] technical term for aerosol extinction coefficient σ_{ex}, expressed in [m^{-1}]

peaks can be seen at geometries 1 and 5. Due to the way the algorithm functions, it wasn't able to properly calculate transmission for the upper layer of clouds, and ended up with a too large value. This is seen in geometry 5, where the simulation radiance offset lies underneath the measured values. To compensate for this, the algorithm reduced transmission in geometry 4, which brought simulated radiance above measured values. Unfortunately, this led to a negative absorption coefficient (physically impossible), which in turn led to a negative peak in the continuum profile at the 4th tangent height, as can be seen in the right graph of Figure 3.2.1 [Höpfner 2002].

A logarithmic retrieval was tried, with the goal of eliminating negative values, but calculations failed with this method. All calculations led to floating point overflows due to near zero values in higher geometries. The compromise was made in the end to accept negative values, which still gave acceptable profiles from a qualitative point of view. Ultimately, 8 iterations were used in the regularisation calculation to make sure the final profile values were stable.

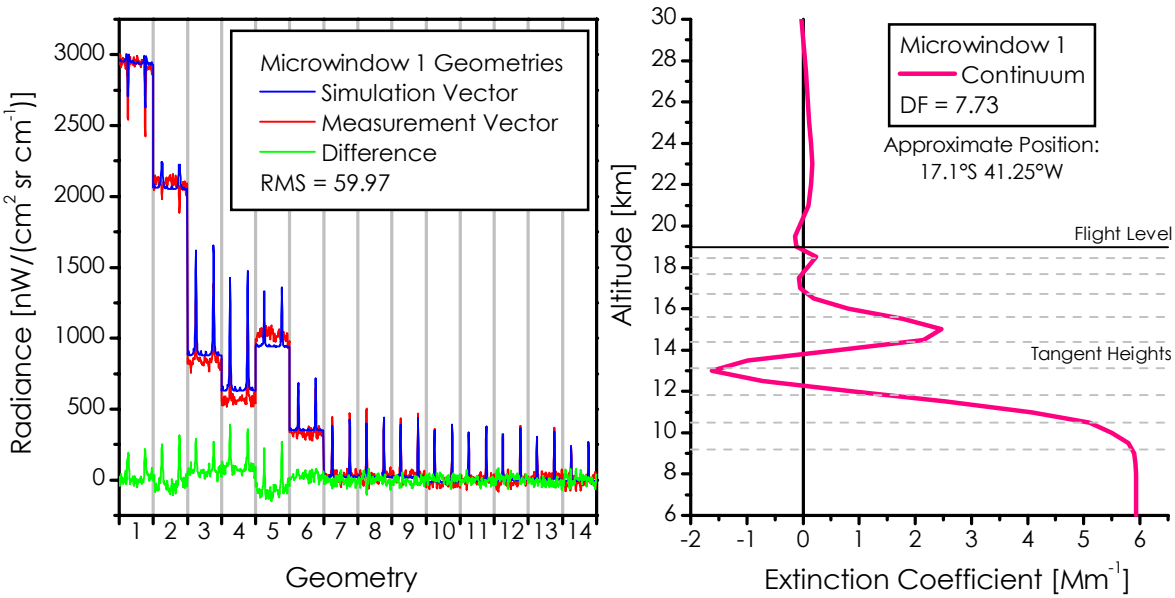

Figure 3.2.1: Example spectral vectors containing geometries for microwindow 1, and corresponding continuum retrieval profile

3.2.2 Results and Observations

Two-dimensional continuum distributions are shown on the next page. Figure 3.2.2 shows results for both flights in full. All tangent geometries were used, except where data was corrupt due to instrument malfunction. This was the case in region 3. Regions 1, 2, 3, and 6 are free of clouds, and have a very limited continuum. Figure 3.2.3 focuses on regions 4 and 5, where clouds were located. The lowest tangent heights that have been plotted are those that were used for temperature and gas retrievals. It is interesting to notice that these geometries follow the cloud envelope. This confirms that no geometries containing clouds were used for the retrieval of other parameters.

What should be noted here is that the quantitative value of these retrievals is not correct, due to the simulation problems mentioned earlier. These could be linked to scattering effects and their simulation by KOPRA, as discussed in [Höpfner, v. Clarmann, and others 2002], or horizontal inhomogeneity of the clouds. Another effect which was not mentioned is the inability to correctly detect continuum below the thicker clouds. This can be seen in Figure 3.2.3 for example where continuum has more or less constant values with height underneath the bottom cloud tops. This is because MIPAS-STR can not see through the clouds, and hence obtains no information from other atmospheric layers. Nevertheless, these plots are clearly successful in terms of locating the upper limit of dense cloud contours, as well as the vertical span of subvisible cirrus clouds (optically thin).

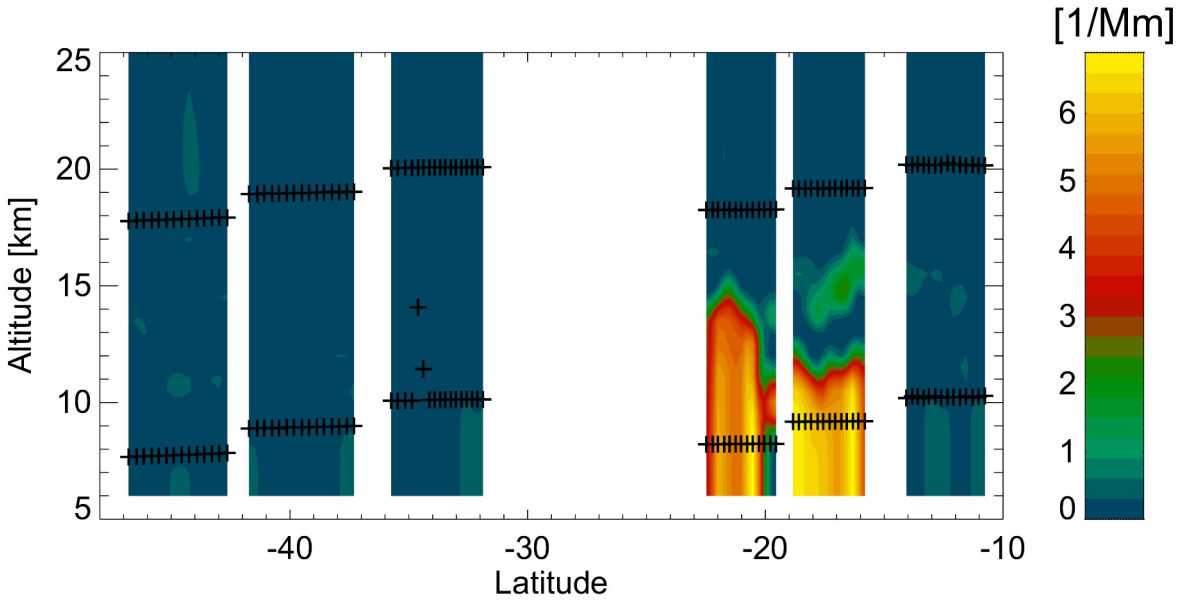

Figure 3.2.2: Two-dimensional distribution of continuum for all flight data

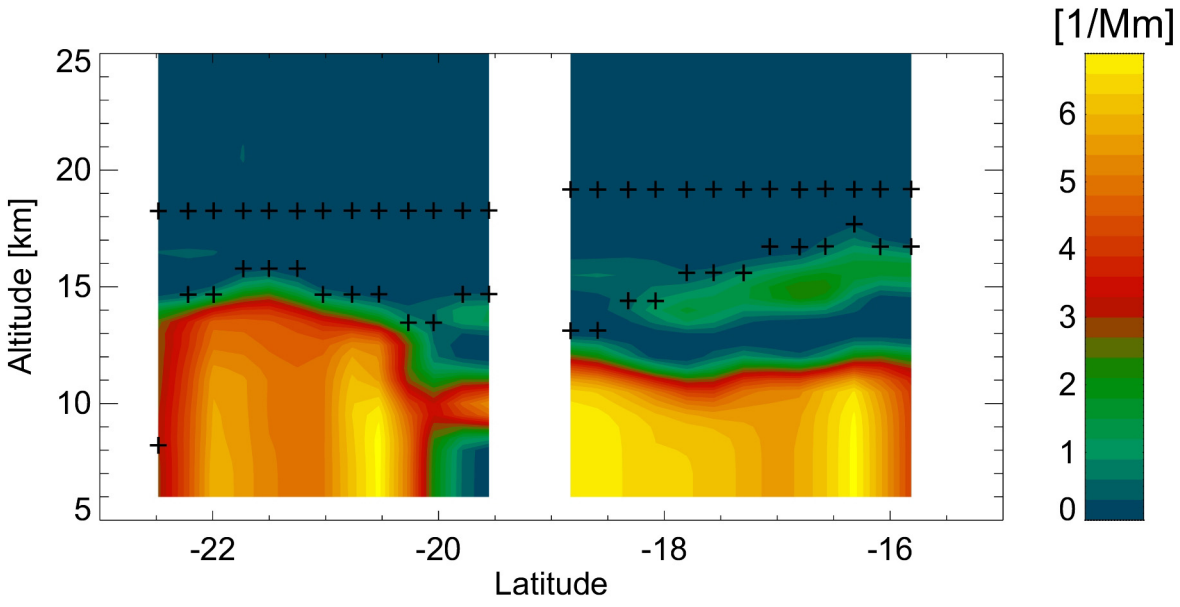

Figure 3.2.3: Two-dimensional distribution of continuum for regions 4 and 5, showing lowest tangent heights used for temperature and gas retrievals

3.3 Nitric Acid (HNO_3)

3.3.1 Calculation Procedures

Three microwindows were used for the retrieval of HNO_3 in ranges between 866 cm^{-1} and 874 cm^{-1}. An existing water line at 871 cm^{-1} was cut out. The resulting spectra were in ranges where no other gas lines were present, which allowed a retrieval of HNO_3 VMR alone. A final value of 3.0×10^7 was chosen for γ_{HNO3}, which confirmed the need for stronger regularisations than for retrievals from other flights (as mentioned for temperature, cf. section 3.1.1). Previously fitted temperature profiles were used for the forward model radiative transfer calculations. Other calculation settings were left as standard. Table 3.3.1 gives a summary of the final settings used for the calculation.

Microwindows [cm^{-1}]	
1	866.0 – 868.0
2	868.0 – 870.5
3	872.0 – 874.0

Fitted Parameters	
HNO_3 VMR	$\gamma_{HNO3} = 3.0 \times 10^7$ (typical DF = 6.7 – 7.0)
shift	(no regularisation)
offset	(no regularisation)

Other Settings	
forward model P-T profiles	interpolated from retrieved temperature from 18-10-1999
regularisation method	Tikhonov-Phillips with constraint to a mid-latitude reference profile shape
regularisation iterations	5

Table 3.3.1: Retrieval parameters for HNO_3

Figure 3.3.1 on the next page shows samples of spectra used for the retrieval calculation of HNO_3. The lines seen here are all from HNO_3. They are not very strong and, therefore, have a quite small SNR[26]. This explains why the difference appears so large between the measured and calculated spectrum. Strong line intensities were not to be expected for these geometries, since HNO_3 is not essentially a tropospheric gas. Its peak concentration lies slightly above the tropopause at about 24 km. At the plotted altitudes, HNO_3 VMR should be close to 0. No considerable difficulties were encountered for HNO_3 retrievals.

[26] Signal-to-Noise Ratio

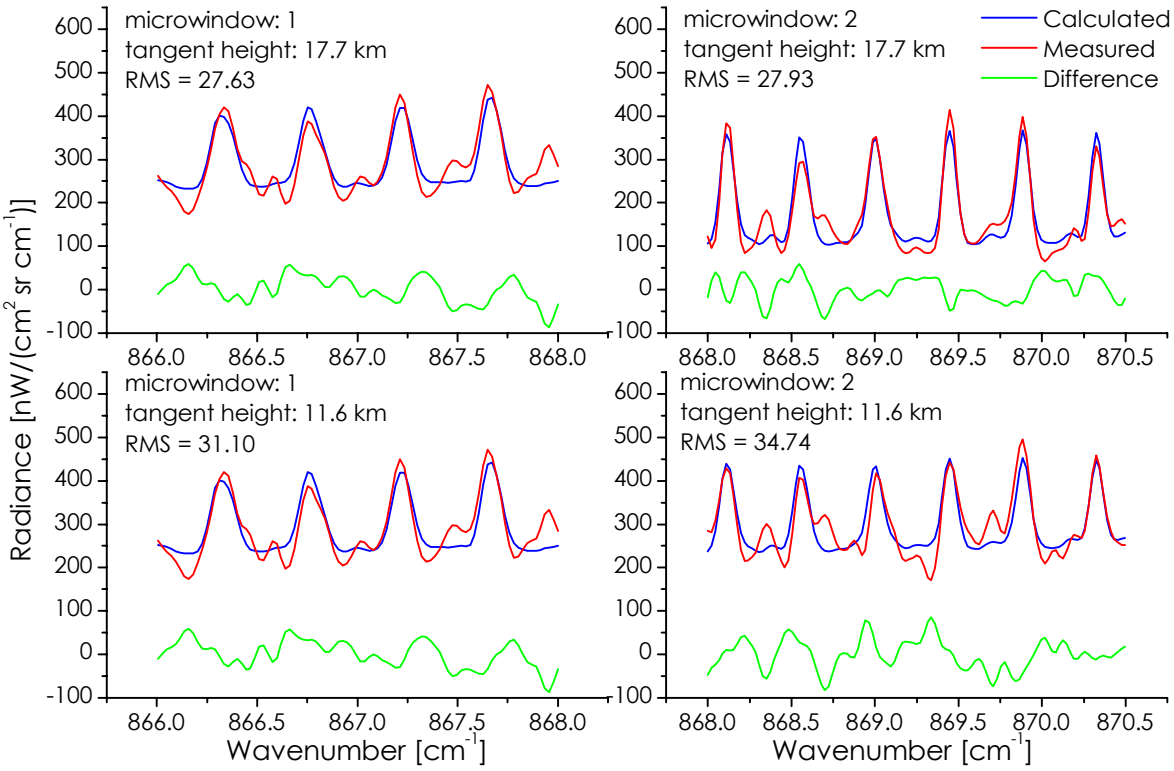

Figure 3.3.1: Sample spectral data for HNO_3 retrieval from microwindows 1 and 2, and geometry tangent heights of 11.6 km and 17.7 km

3.3.2 Results and Observations

Figure 3.3.2 is a sample retrieved profile from region 1. The profile in Figure 3.3.3 is from region 6 and corresponds to the sample spectra shown in Figure 3.3.1. As said before, HNO_3 has a limited concentration within the troposphere. However, concentrations in region 6 appear to be much lower than the reference profile. This is not exactly true. It was noted for the temperature retrievals (cf. Figure 3.1.4) that the troposphere rose as the equator was approached, which implies an upward shift in gas profiles as well. The reference profile used for the fit was a mid-latitude profile, calibrated for the beginning of the flights, so this leads to the conclusion that HNO_3 VMR is in not smaller, but simply shifted in altitude. Noteworthy is the value of this shift, measured here to be about 4 km, which corresponds exactly with the value noted for temperature. When the retrieval is compared to the standard equatorial profile, it fits much better.

This shift in the profile of region 6 was not well retrieved for geometries above the aircraft. This is expectable, as there is much less information available from that portion of the atmosphere. Consequently, profiles have a much stronger tendency to follow the reference profile shape during the regularisation process. This effect is clearly visible for the portion of this profile above the flight level. The same effect can be noted underneath the lowest tangent height, although for HNO_3 this is not important, due to near constant concentrations in those altitudes. For other gases though, this may have a more noticeable influence on profile shapes.

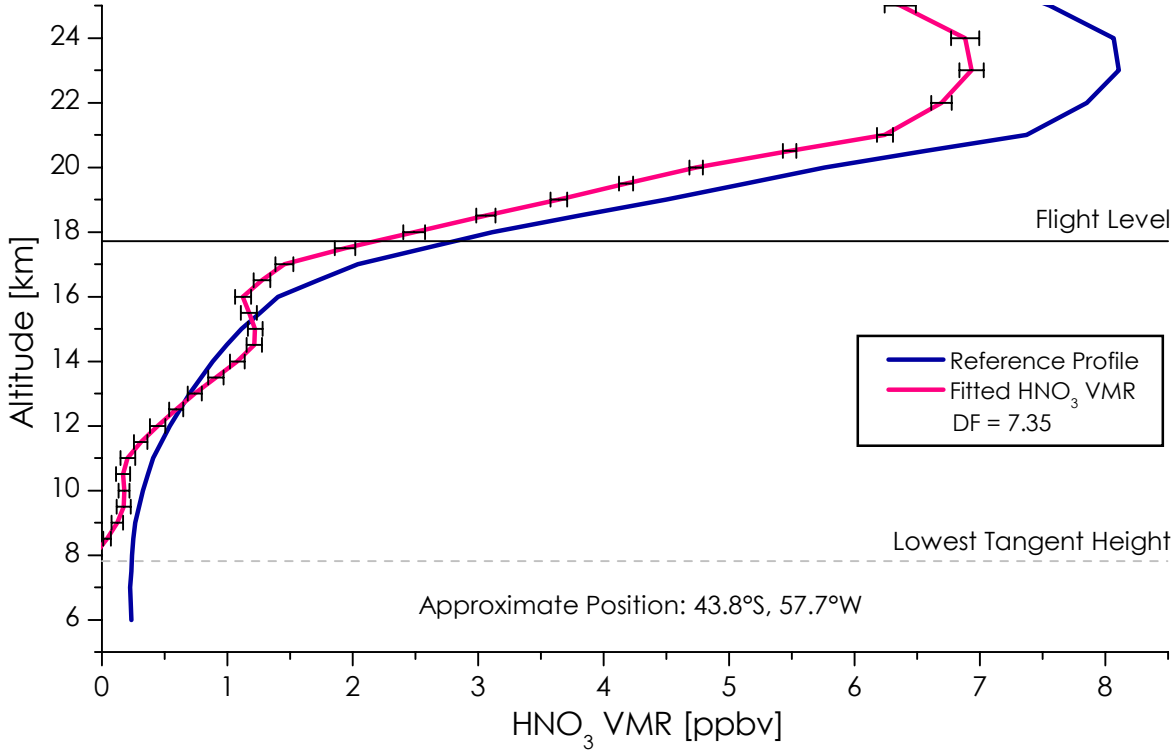

Figure 3.3.2: Retrieved HNO_3 profile from region 1 with NESR error and initial guess

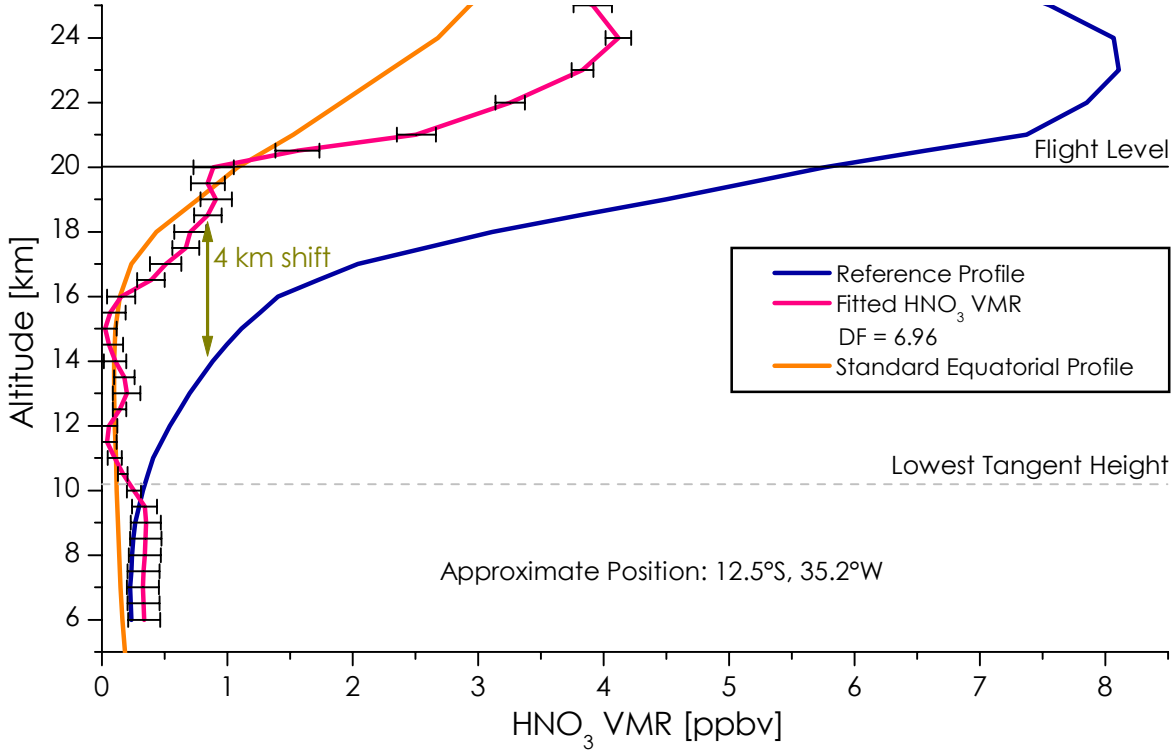

Figure 3.3.3: Retrieved HNO_3 profile from region 6 with NESR error, initial guess, and standard equatorial profile (not used for the retrieval)

Figure 3.3.4 shows the linearly interpolated retrieval result for HNO_3 VMR, which is near 0 in the troposphere, and rises to a maximum of about 8 ppbv in the lower stratosphere at about 24 km. Above this level, HNO_3 is eliminated through photolysis by solar radiation. The limit of the troposphere is quite visible here at 12 km at low latitudes, and 16-17 km near the equator. What should be noted here is the quality of the retrieval, as can be seen in regions 1 to 3. Although the flight altitude changes significantly between the three, the concentration distributions of these three regions are coherent.

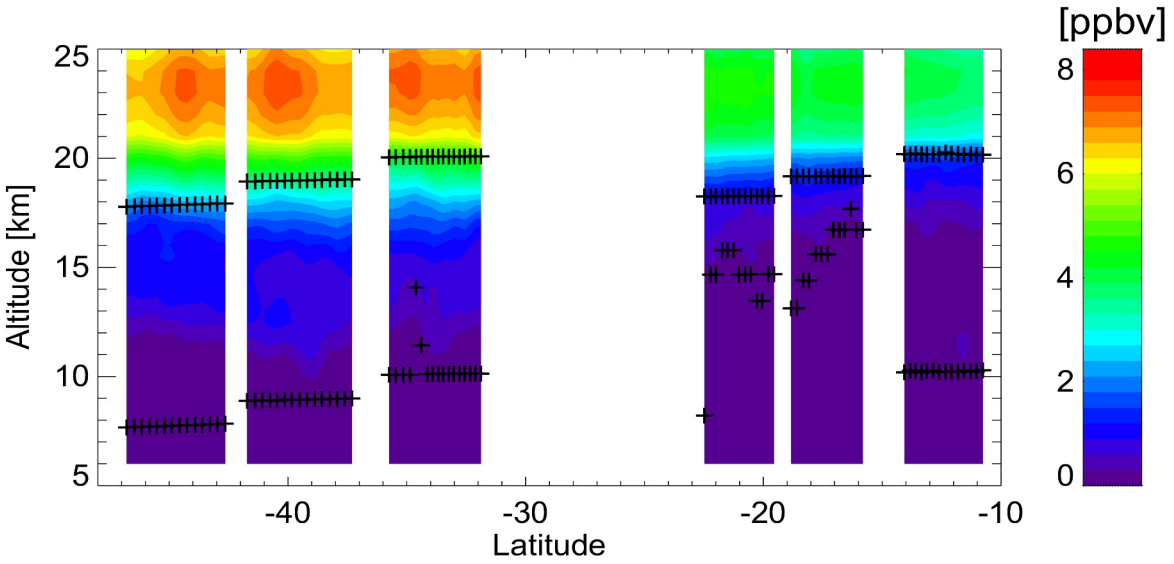

Figure 3.3.4: Two-dimensional distribution of retrieved HNO_3 VMR

3.3.3 Comparison with KASIMA Model Results

A comparison with the KASIMA[27] chemical transport model results is quite good. The VMR gradient is visible here as well and is similar to the retrieval results. One must just note that the KASIMA results only go up to 20 km, and have a horizontal resolution of 5°, which explains why no small scale features are visible.

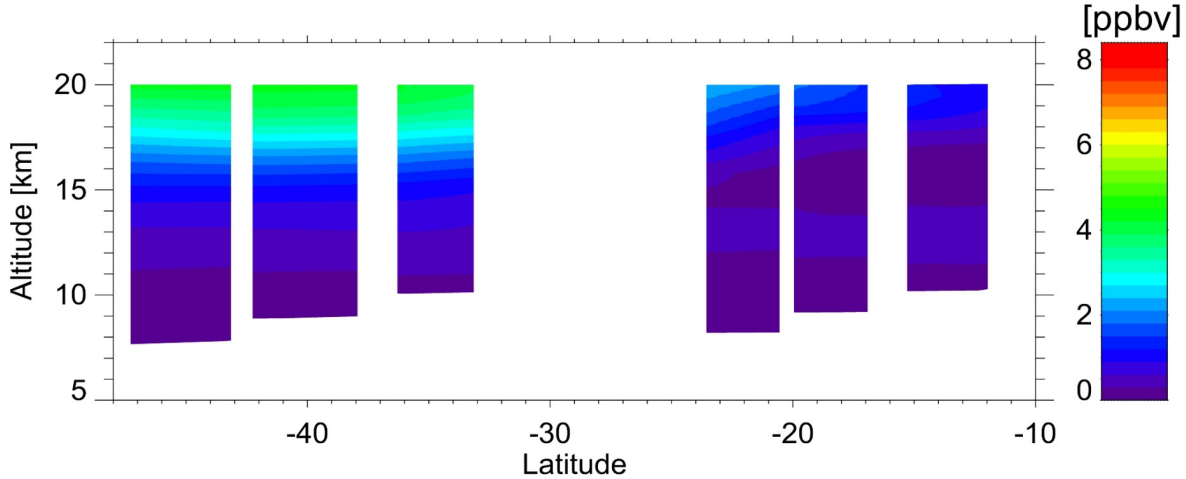

Figure 3.3.5: Two-dimensional distribution of HNO_3 VMR from the KASIMA model

[27] KArlsruhe SImulation model of the Middle Atmosphere

3.4 Chlorine Nitrate ($ClONO_2$)

3.4.1 Calculation Procedures

Only one microwindow was used for the retrieval of chlorine nitrate, between 779.5 cm^{-1} and 781.0 cm^{-1}. O_3 and CO_2 also have spectral lines in this interval which meant that $ClONO_2$ could not be retrieved on its own. O_3 was included in the regularisation process, in order to minimise any influence on the $ClONO_2$ retrieval. This was not necessary for CO_2, as its profile is already quite precisely known. The final retrieval settings are shown in Table 3.4.1

Microwindows [cm^{-1}]	
1	779.5 – 781.0

Fitted Parameters	
$ClONO_2$ VMR	γ_{ClONO2} = 7.5 x 10^8 (typical DF = 4.6 – 5.3)
O_3 VMR	γ_{O3} = 50.0 (typical DF = 5.9 – 6.9)
shift	(no regularisation)
offset	(no regularisation)

Other Settings	
forward model P-T profiles	interpolated from retrieved temperature from 18-10-1999
regularisation method	Tikhonov-Phillips with constraint to a mid-latitude reference profile shape
regularisation iterations	5

Table 3.4.1: Retrieval parameters for $ClONO_2$

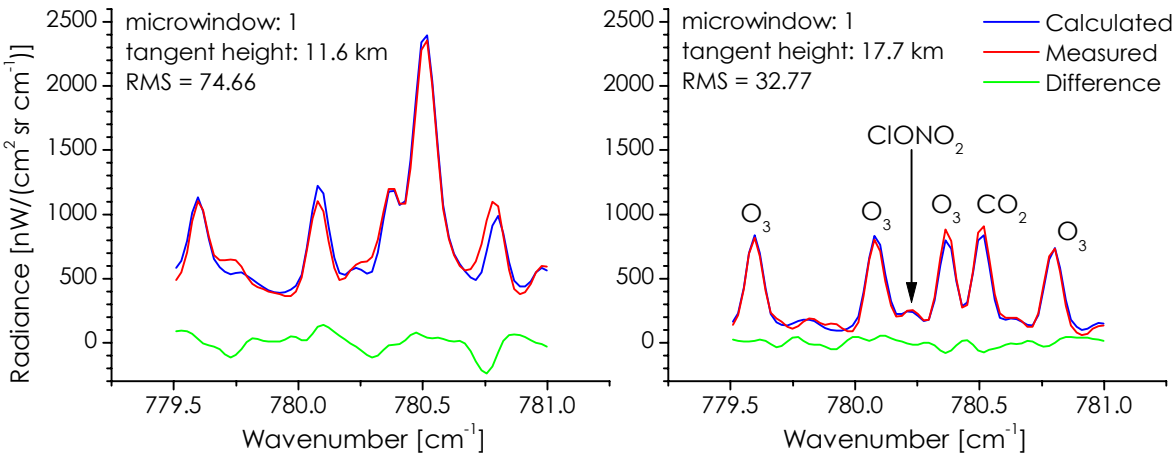

Figure 3.4.1: Sample spectral data for $ClONO_2$ retrieval from geometry tangent heights of 11.6 km and 17.7 km

Figure 3.4.1 shows a sample of the spectra, from two different tangent heights, which was used for the retrieval calculations. On the higher tangent height graph the spectal lines have been identified for the different gases present. As can be seen, the $ClONO_2$ signature is quite small compared to surrounding O_3 lines, which justifies the need to include the latter in the inversion calculation.

The fact that the spectral signature for chlorine nitrate is so small led to some problems with the retrieval calculations. As noted earlier, the spectral data from 18 October 1999 contained noticeably more noise than data from other flights. This spectral noise meant that the SNR for the concerned line was quite poor, and consequently led to quite unstable profiles (cf. section 2.4.3). In 3 cases, the spectral noise was in fact so important that the scan geometries had to be removed from calculations altogether. The remaining data was fitted with strong regularisation parameters in an attempt to obtain smoother results. Unfortunately, this was done at the cost of a stronger correspondence with reference profiles.

3.4.2 Results and Observations

The retrieved $ClONO_2$ VMR profiles seen in Figure 3.4.2 and Figure 3.4.3 have some similarities with HNO_3, although the peak in concentration is somewhat higher in the stratosphere. The retrieval for the present gas did not give as good results, however, since portions of the profile within the limits of the lowest and flight level tangent heights are negative, which is evidently impossible. This can be explained by the fact that concentrations there are near zero, and hence have spectral measurements with poor SNRs. This is made worse by the high level of noise in the spectra as mentioned earlier, which is confirmed in the graphs, where error bars appear much larger than in HNO_3. For areas with higher concentrations this does not appear to be as much of a problem, such as in the profile of region 6, which follows the standard equatorial profile quite well above 0.1 ppbv.

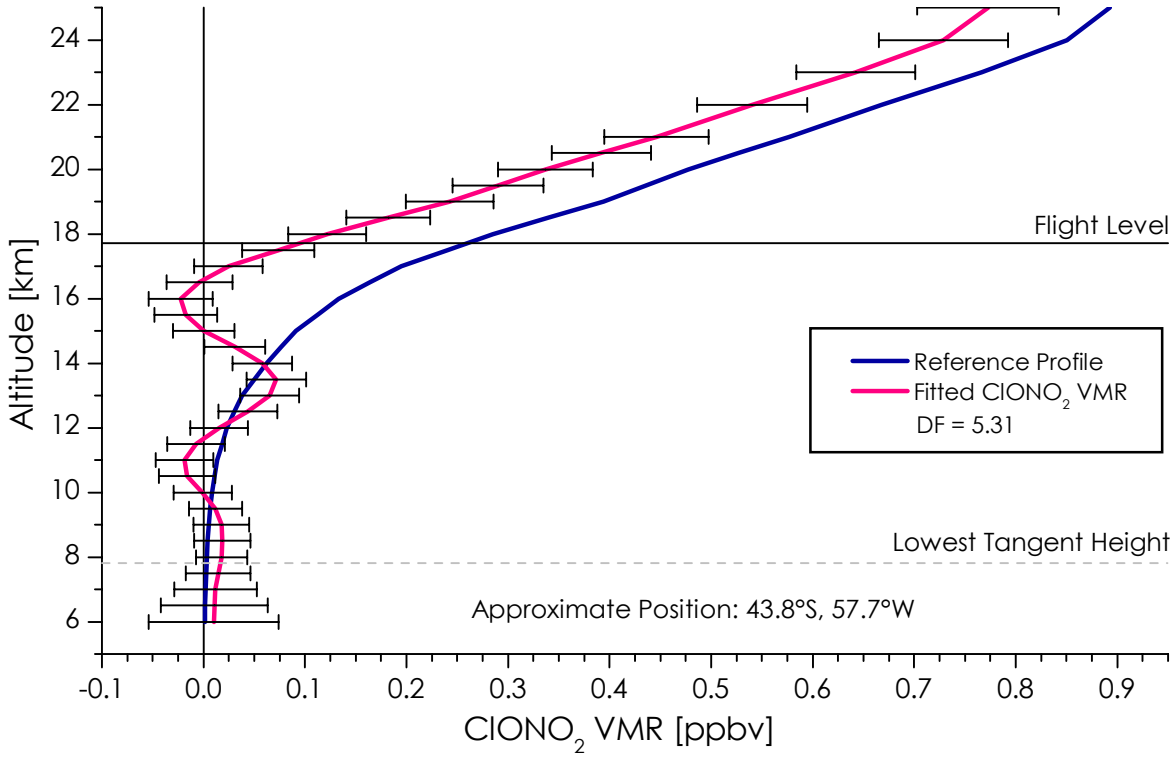

Figure 3.4.2: Retrieved $ClONO_2$ profile from region 1 with NESR error and initial guess

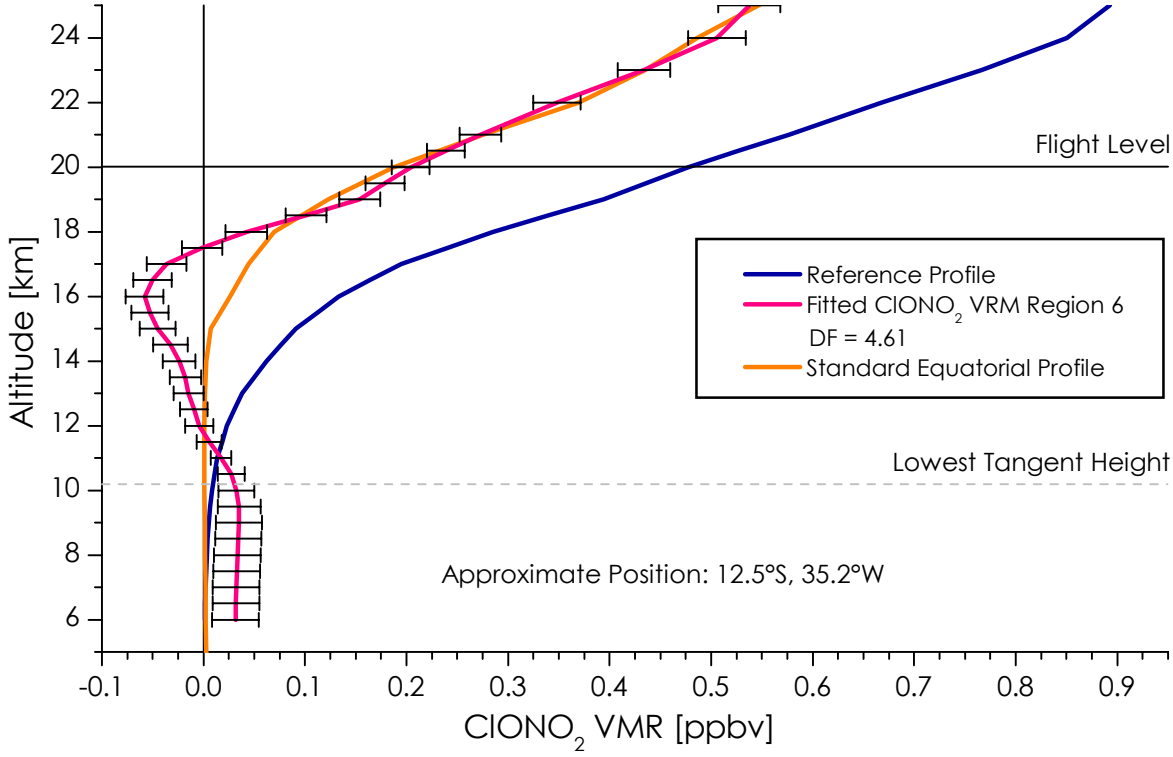

Figure 3.4.3: Retrieved $ClONO_2$ profile from region 6 with NESR error, initial guess, and standard equatorial profile (not used for the retrieval)

Figure 3.4.4 shows the final retrieval of $ClONO_2$. The difficulty in obtaining stable profiles can be seen here with the slightly unstable concentration gradient. Plotted here is a linear interpolation of the individual profiles, which smoothed out these irregularities to some extent. Negative concentrations have all been eliminated here and have been replaced by null values. What can be said is that although this retrieval proved to be slightly trickier than nitric acid, we still obtained a good coherence between the different regions, and the rise of the troposphere is still clearly visible.

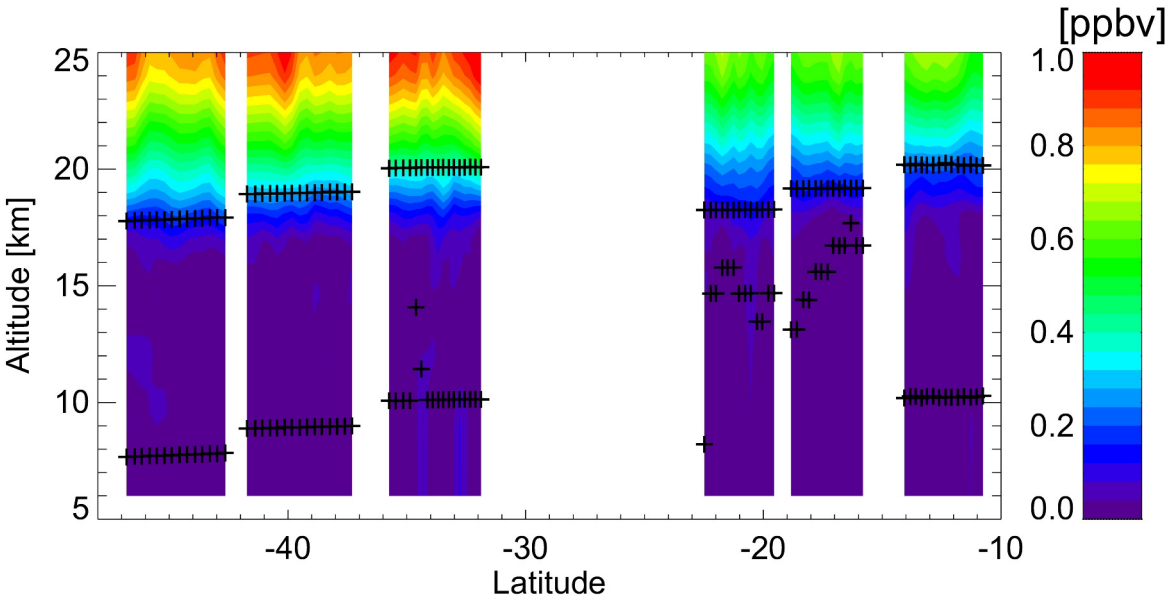

Figure 3.4.4: Two-dimensional distribution of retrieved $ClONO_2$ VMR

3.5 Ozone (O_3)

3.5.1 Calculation Procedures

Ozone was retrieved using 10 microwindows within the 782.5 – 813.7 cm^{-1} spectral range. CCl_4 also has signatures for these wavenumbers, so it was necessary to include it in the regularisation calculations. Values for γ_{CCl4} and γ_{O3} were set to 5.0 x 10^9 and 75.0 respectively, once again confirming the need for a stronger regularisation than for other flights. As before, default settings were used for other calculation parameters. A summary is shown in Table 3.5.1.

Microwindows [cm^{-1}]	
1	782.5 – 783.5
2	785.3 – 786.5
3	787.0 – 788.0
4	788.5 – 789.6
5	794.2 – 795.2
6	795.5 – 795.9
7	804.9 – 806.0
8	806.5 – 807.6
9	811.1 – 812.3
10	812.7 – 813.7

Fitted Parameters	
CCl_4 VMR	γ_{CCl4} = 5.0 x 10^9 (typical DF = 2.4 – 2.9)
O_3 VMR	γ_{O3} = 75.0 (typical DF = 6.6 – 7.6)
shift	(no regularisation)
offset	(no regularisation)

Other Settings	
forward model P-T profiles	interpolated from retrieved temperature from 18-10-1999
regularisation method	Tikhonov-Phillips with constraint to a mid-latitude reference profile shape
regularisation iterations	5

Table 3.5.1: Retrieval parameters for O_3

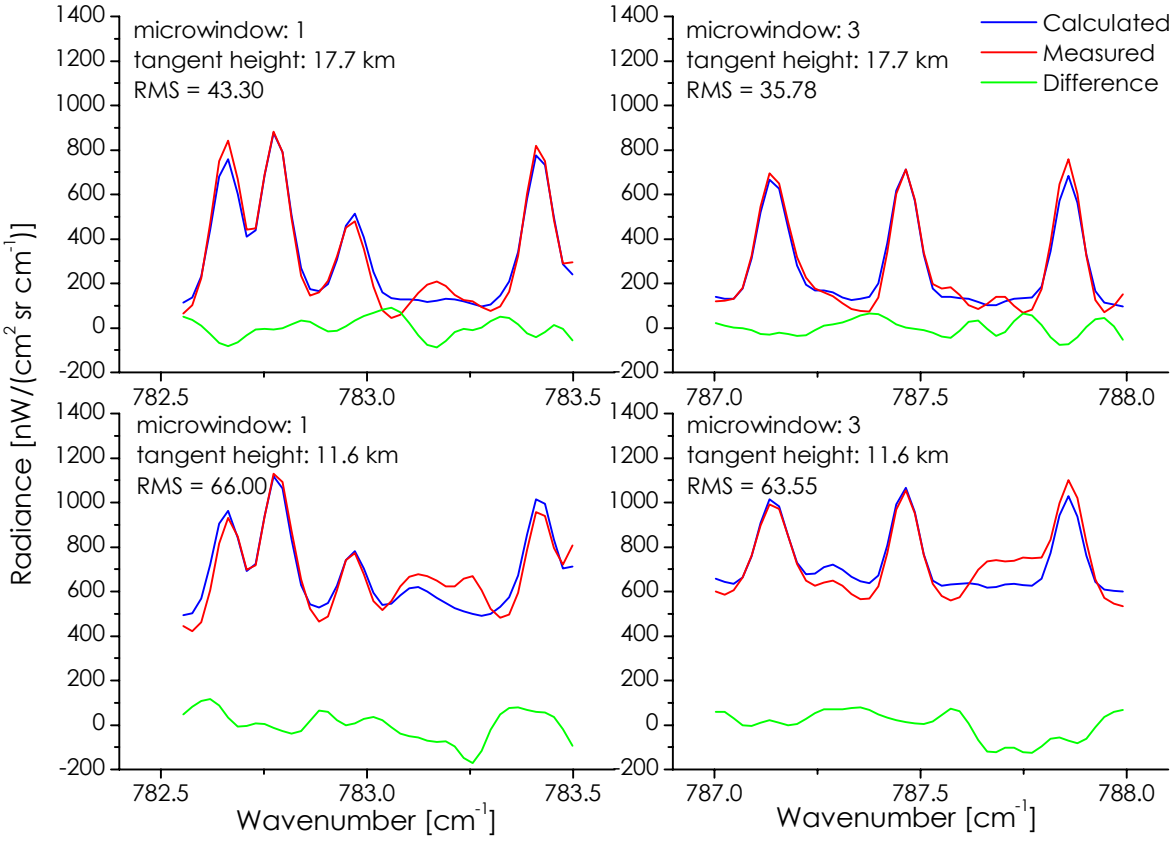

Figure 3.5.1: Sample spectral data for O_3 retrieval from microwindows 1 and 3, and geometry tangent heights of 11.6 km and 17.7 km

Spectra samples from microwindows 1 and 3 are shown in Figure 2.1.1 for two tangent heights. The lower tangent heights show a much stronger background radiation than the upper ones. This is in fact mostly CCl_4 signature [Echle 1992], which is why this gas needed to be included in the inversion calculations.

Ozone is yet another stratospheric gas, for which concentrations at and under flight level are near null. Ozone retrieval proved more straightforward, however, than $ClONO_2$, since the quantity and intensity of available spectral lines was considerably bigger. This helps KOPRAFIT fit the spectral vector to its measured counterpart in a much more precise manner during the regularisation calculation.

As a result, the retrieved profiles seemed less sensitive to changes in γ_{O3}, thus reducing the amount of test calculations necessary to determine an acceptable value for the parameter. This being said, however, since most of the atmospheric layers containing O_3 were situated above the aircraft, it was difficult to know whether profile shape for areas with substantial traces of the gas were trustworthy.

3.5.2 Results and Observations

Figure 3.5.2 shows a retrieved O_3 VMR profile from region 1. The NESR error appears to be clearly smaller here than with HNO_3 and $ClONO_2$. As stated before, this is most likely linked to stronger spectral lines, as well as the higher number of available spectral intervals to work with. Consequently, problems such as negative values at low concentrations as seen with $ClONO_2$ (cf. Figure 3.4.2 and Figure 3.4.3) are more or less eliminated. The retrieved profile here does swings a bit about the initial guess profile between 10 km and 12 km, but this is probably simply linked to a high value of DF. On average, parameter retrievals were achieved with DF values of about 6.5 – 7, whereas here the value is 8.08. Nevertheless, the profile seems to follow the initial guess at low altitudes. It should be noted that above 18 km the concentration gradient is noticeably larger than the initial guess.

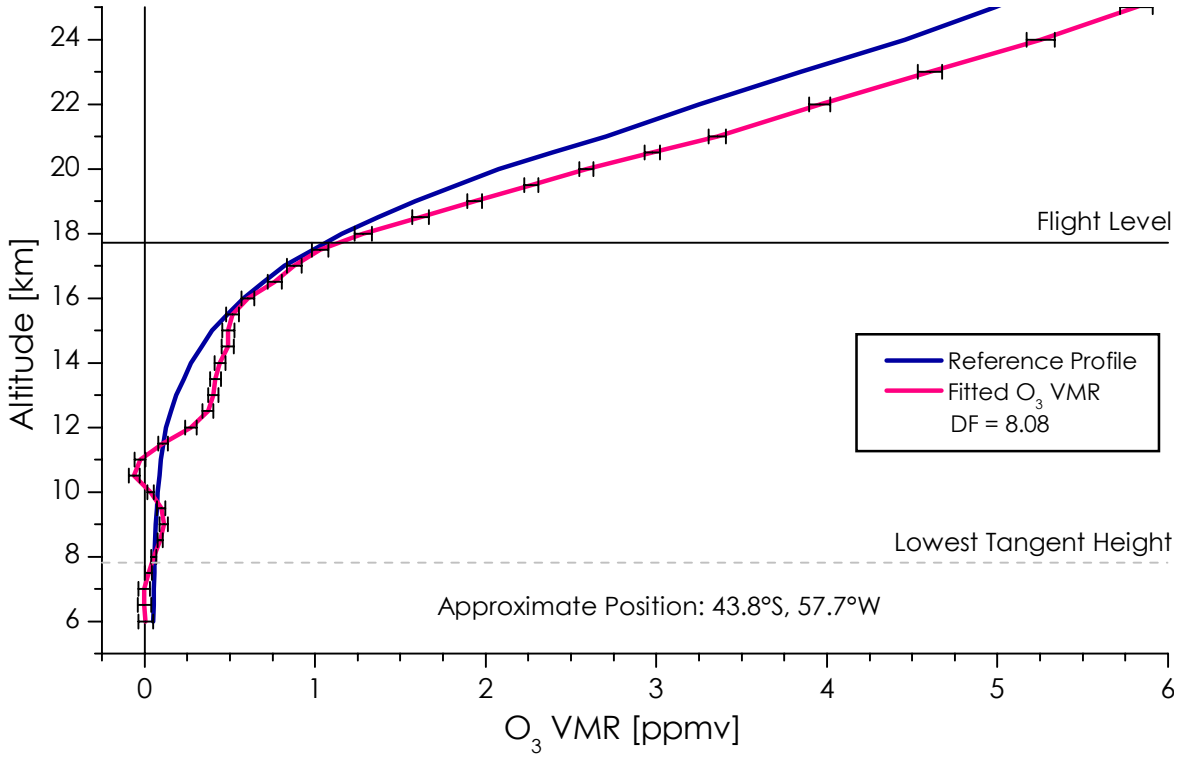

Figure 3.5.2: Retrieved O_3 profile from region 1 with NESR error and initial guess

Figure 3.5.3 on the next page shows a sample retrieval profile from region 6, which corresponds to the spectra seen in Figure 3.5.1. The previous remarks concerning NESR error and low concentration profile shapes apply here as well. As noticed with the previous parameter retrievals, a vertical shift region 6 seems present, but this time the comparison to a standard equatorial profile is not as good. For some reason above 17 – 18 km, just as noticed in Figure 3.5.2, the concentration gradient is higher than for the reference profiles and a clear divergence from the latter is visible. This is in fact the case for all the profiles of this retrieval. A preliminary comparison to data from other experimental instruments suggested that this higher VMR could be erroneous. Unfortunately, this could not be confirmed, as more work is required to carry out a rigorous comparison.

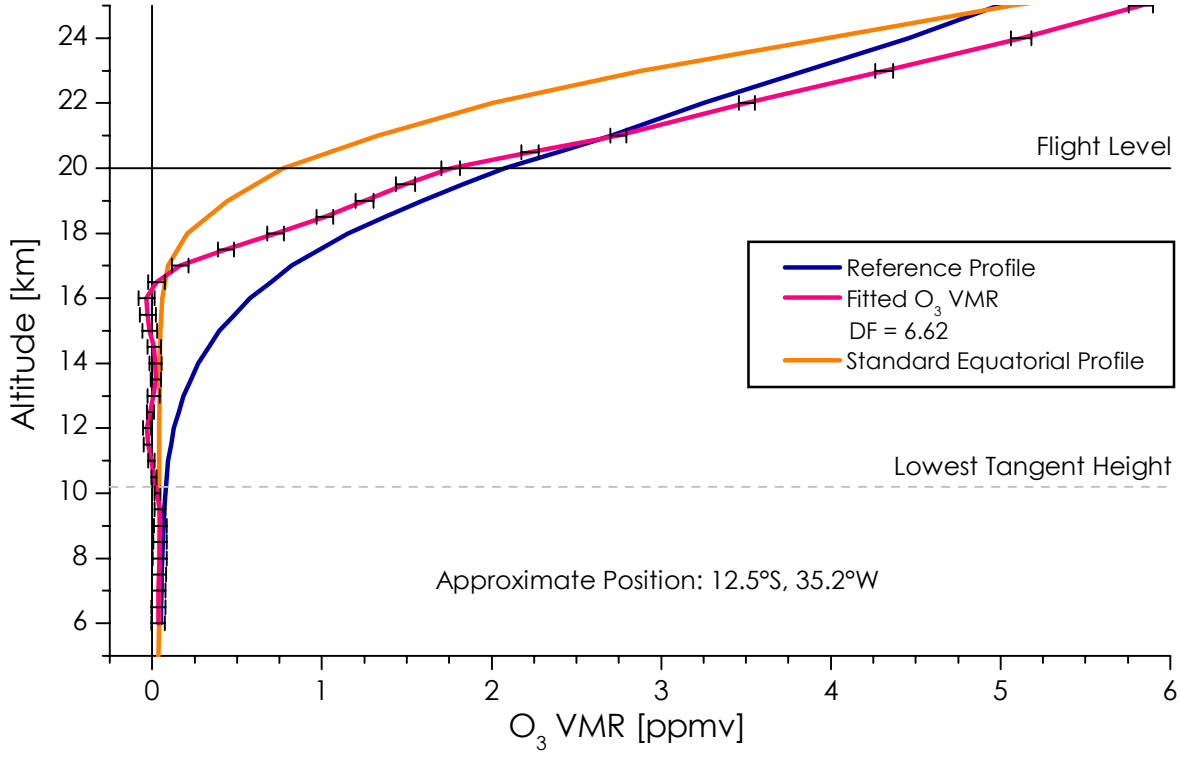

Figure 3.5.3: Retrieved O_3 profile from region 6 with NESR error, initial guess, and standard equatorial profile (not used for the retrieval)

The retrieved two dimensional distribution of O3 VMR is shown in Figure 3.5.4. It is important to note here that a rise in the tropopause is not clearly visible. This is the only parameter retrieval where this is the case, which is a further strong hint to a possible erroneous fit in higher altitudes. To be sure of this, further work including simulations and more data analysis would have needed to be done. This, however, was beyond the scope of the present work.

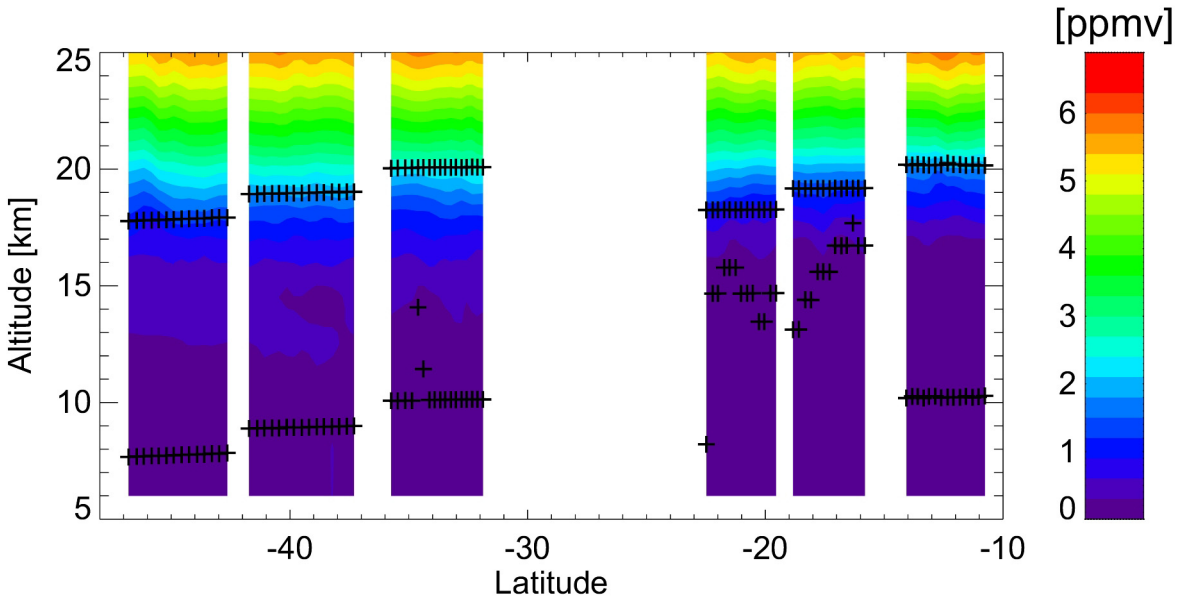

Figure 3.5.4: Two-dimensional distribution of retrieved O_3 VMR

3.6 Trichlorofluoromethane, CFC-11 (CCl_3F)

3.6.1 Calculation Procedures

Calculation settings for the retrieval of CFC-11 were trickier to establish than for other gases, and several standard parameters were changed in an attempt to obtain better results. One microwindow was used for this retrieval, with a wide wavenumber range due to this gas's broad spectral signature. Several water vapour lines are present in this microwindow as well, which required the inclusion of H_2O in the retrieval process. Both gases were strongly regularised, so as to compensate for retrieval profiles which proved quite unstable. In a further attempt to better the results, two settings were changed in KOPRA. The extra FOV geometries setting for ray tracing calculations was increased from 5 to 9. Phosgene, which may have signatures for some geometries in this microwindow was added in the radiative transfer calculations. A summary of the final settings used is shown in Table 3.6.1.

Microwindows [cm^{-1}]	
1	838.0 – 856.0

Fitted Parameters		
H_2O VMR	γ_{H2O} = 0.10	(typical DF = 5.0 – 6.2)
CFC-11 VMR	γ_{CFC11} = 1.0 x 10^{10}	(typical DF = 5.7 – 6.7)
shift	(no regularisation)	
offset	(no regularisation)	

Other Settings	
forward model P-T profiles	interpolated from retrieved temperature from 18-10-1999
extra forward model gas	Phosgene ($COCl_2$)
forward model FOV, extra geometries	9
regularisation method	Tikhonov-Phillips with constraint to a mid-latitude reference profile shape
regularisation iterations	5

Table 3.6.1: Retrieval parameters for CFC-11

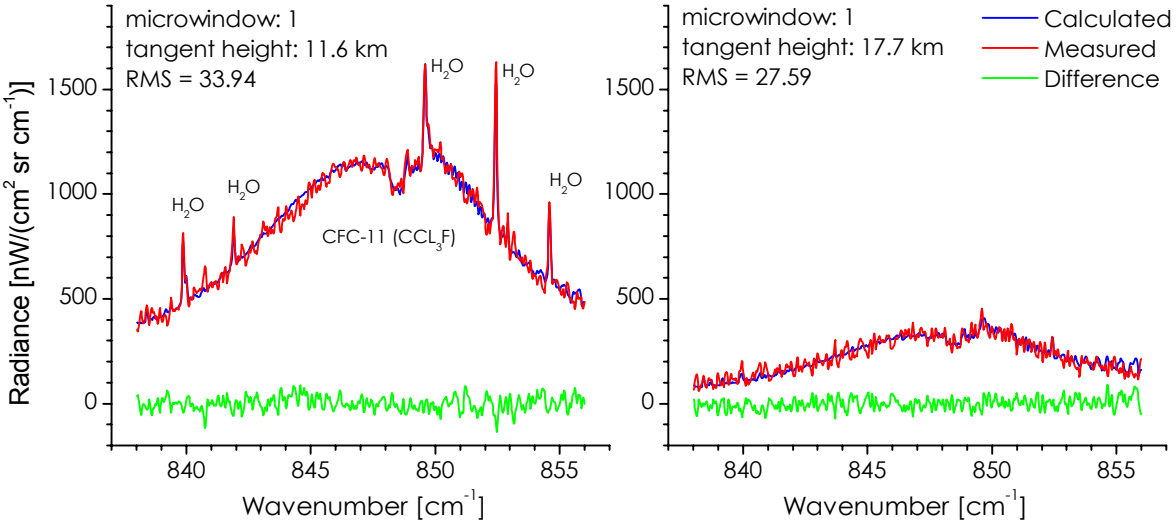

Figure 3.6.1: Sample spectral data for CFC-11 retrieval from geometry tangent heights of 11.6 km and 17.7 km

Sample spectra used in the final retrieval calculations are shown in Figure 3.6.1. Water vapour lines can be clearly seen in the lower geometry. Unlike microwindows from the previously discussed retrievals, the one used here is quite large, which offers a different view of the spectra. Noise, mentioned several times earlier, is clearly seen here. Although the measurement spectrum envelope follows the calculated spectrum quite well, there is a strong random fluctuation about it. This is obviously unwanted for good retrieval calculations.

The first series of test calculations used common settings, notably the inclusion of HNO_3 in the retrieval, and a microwindow range of 840 – 860 cm^{-1}. It was quickly noticed that something was not working well in the calculations, and which was causing the VMR at low altitudes to increase to abnormal values of roughly 5 times the reference profile as can be seen in Figure 3.6.2 on the next page. This was evidently not possible since gas concentrations are by definition practically constant in the troposphere. A look at the resulting spectral vectors showed that HNO_3 on the right side of the microwindow was not being properly fitted, as well as the various water lines present. This can be seen in the sample of bad spectra in Figure 3.6.2 and is emphasised by the large RMS value.

The decision was made to change the microwindow range (cf. Table 3.6.1, and Figure 3.6.1) to minimise the influence of HNO_3 signature, and to properly include an H_2O line at 840 cm^{-1}. HNO_3 was no longer included in the retrieval, and H_2O on the contrary was added. Two additional settings were changed in the forward model, as mentioned earlier. These changes from common procedure proved somewhat beneficial, although a quite strong regularisation was still needed in the end to stabilise the profiles. Regularisation parameters γ_{H2O} and γ_{CFC11} were chosen in order to obtain average profile DF values of 6.

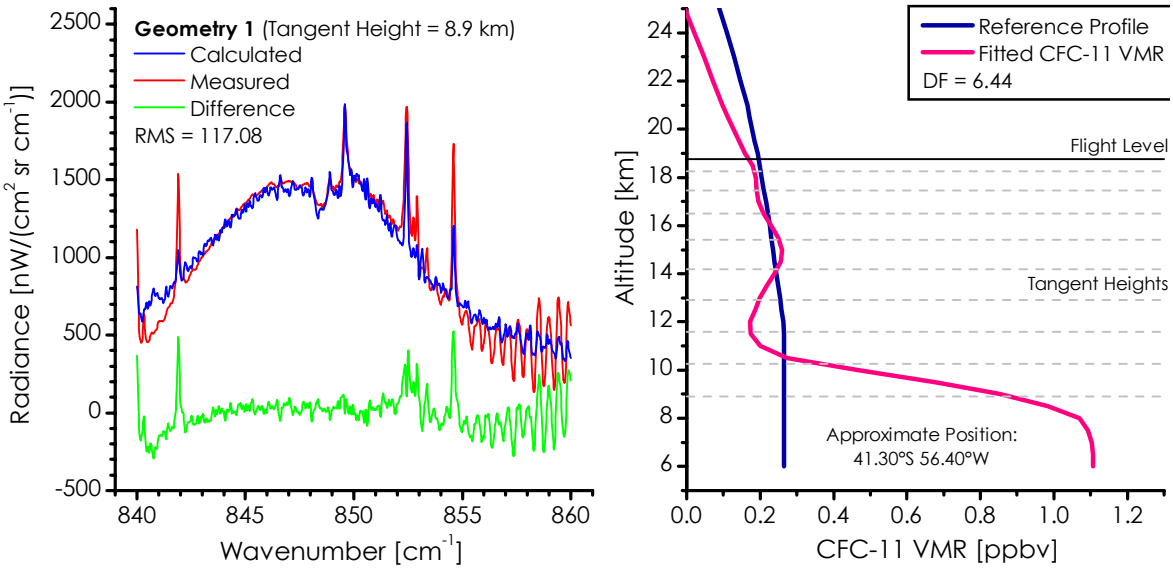

Figure 3.6.2: Bad retrieval example from first test-run series for CFC-11, with sample spectra from region 2 for lowest geometry and corresponding retrieved profile

3.6.2 Results and Observations

Profiles from region 1 and 6 are shown respectively in Figure 3.6.3, and Figure 3.6.4 on the next page. In both cases, the fit does not follow the reference profile particularly well. In region 6, the comparison to the standard equatorial profile isn't better. This could simply be because the gas VMRs are truly different. However, profile minimums at lower altitudes – although the DF values are small – hint to another factor, namely strong noise and in low altitudes aerosol absorption.

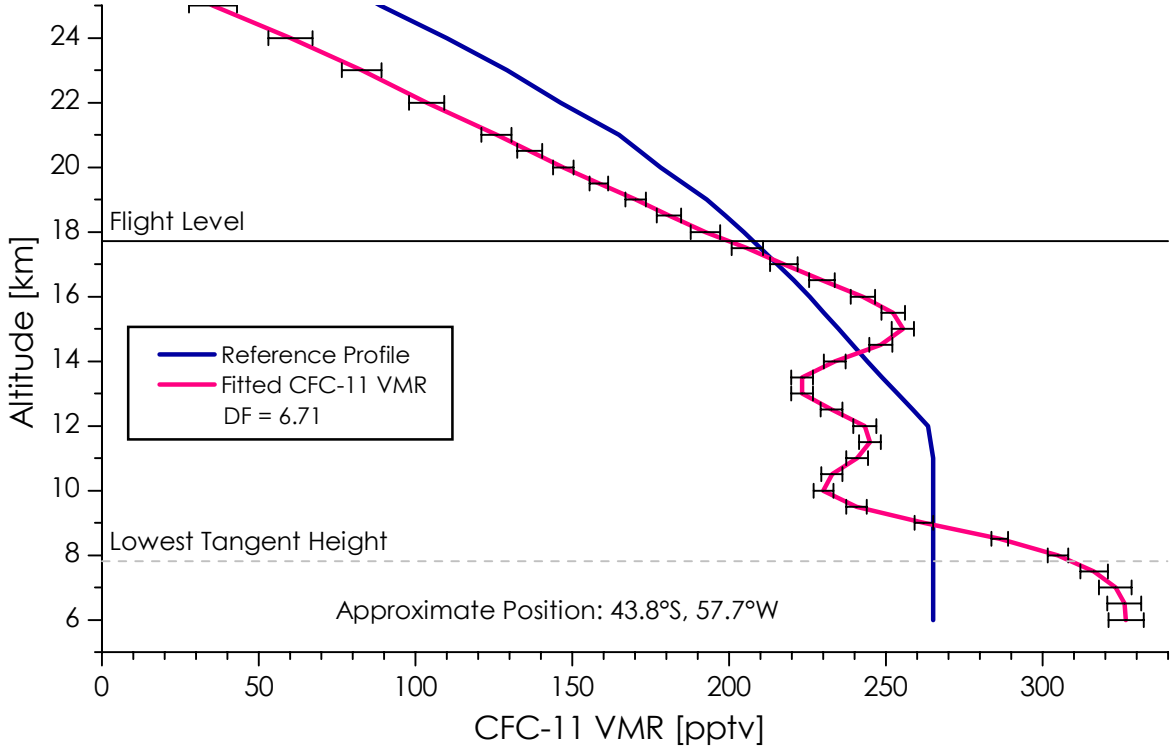

Figure 3.6.3: Retrieved CFC-11 profile from region 1 with NESR error and initial guess

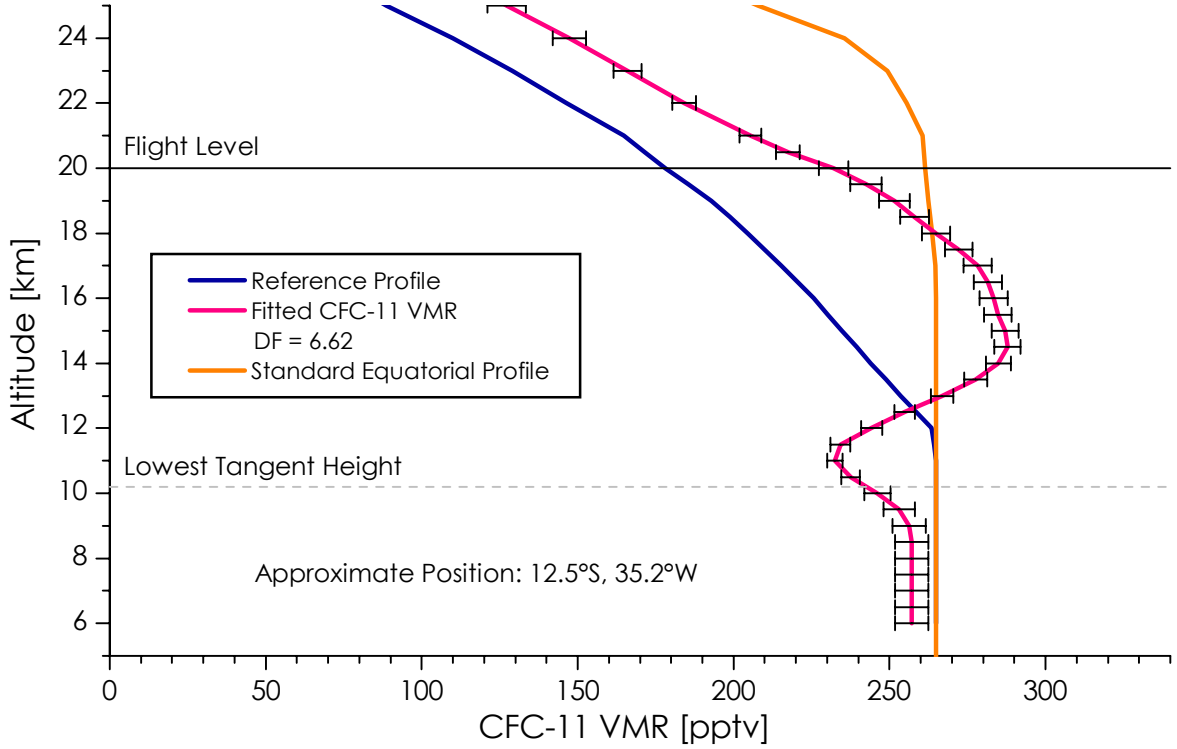

Figure 3.6.4: Retrieved CFC-11 profile from region 6 with NESR error, initial guess, and standard equatorial profile (not used for the retrieval)

Figure 3.6.5 shows the retrieved distribution of CFC-11 VMR. The retrieval difficulties can be seen in several ways. Minimums in the troposphere in regions 1-3 are almost certainly erroneous, and are due to profile oscillations. White regions are due to unlikely high VMRs values. Finally, the tropopause in regions 4-6 follows the flight level quite precisely, which was not seen in the previously discussed retrievals. This too could be linked to incorrect calculations.

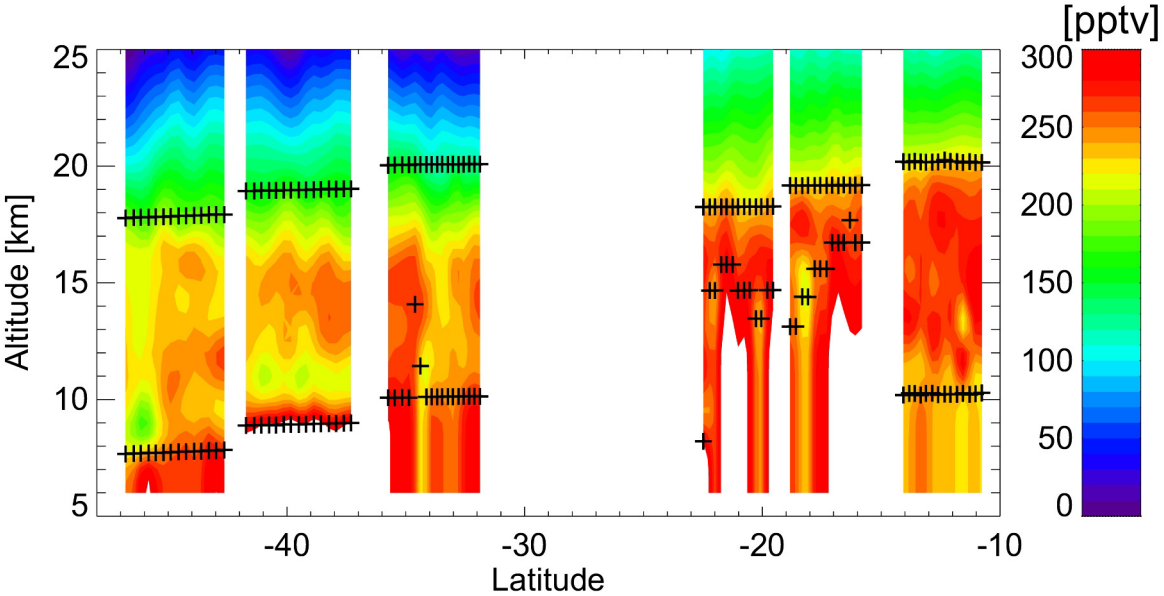

Figure 3.6.5: Two-dimensional distribution of retrieved CFC-11 VMR

3.7 Dichlorodifluoromethane, CFC-12 (CCl_2F_2)

3.7.1 Calculation Procedures

CFC-12 was retrieved with 1 microwindow in the wavenumber range of 920.5 – 924.0 cm^{-1}. Some CO_2 spectral lines are present here, as well as an H_2O spectral line at about 922.15 cm^{-1}. Consequently, water vapour was included in the retrieval calculations. An HNO_3 background is also present, but a test run showed that it was better not to fit this gas. As for CFC-11, difficulties were encountered during the retrieval of this gas. Two different calculation methods were used in the end, both showing their advantages. The first retrieval method used an offset fit to correct offsets in the spectra, whereas in the second method these were corrected with a continuum fit. All regularisation parameters were chosen to force DF values to about 5. A summary of the parameter settings for both retrieval methods is given in Table 3.7.1.

Microwindows [cm^{-1}]	
1	920.5 – 924.0

Fitted Parameters (offset fit)	
H_2O VMR	γ_{H2O} = 2.35 x 10^{-3} (typical DF = 4.3 – 5.6)
CFC-12 VMR	γ_{CFC12} = 2.1 x 10^{9} (typical DF = 4.5 – 5.3)
shift	(no regularisation)
offset	(no regularisation)

Fitted Parameters (continuum fit)	
continuum	γ_{con} = 5.1 x 10^{9} (typical DF = 4.9 – 5.5)
H_2O VMR	γ_{H2O} = 2.1 x 10^{-3} (typical DF = 4.2 – 5.8)
CFC-11 VMR	γ_{CFC11} = 5.3 x 10^{9} (typical DF = 4.6 – 5.7)
shift	(no regularisation)

Other Settings	
forward model P-T profiles	interpolated from retrieved temperature from 18-10-1999
forward model FOV, extra geometries	9
regularisation method	Tikhonov-Phillips with constraint to a mid-latitude reference profile shape
regularisation iterations	5

Table 3.7.1: Retrieval parameters for CFC-12

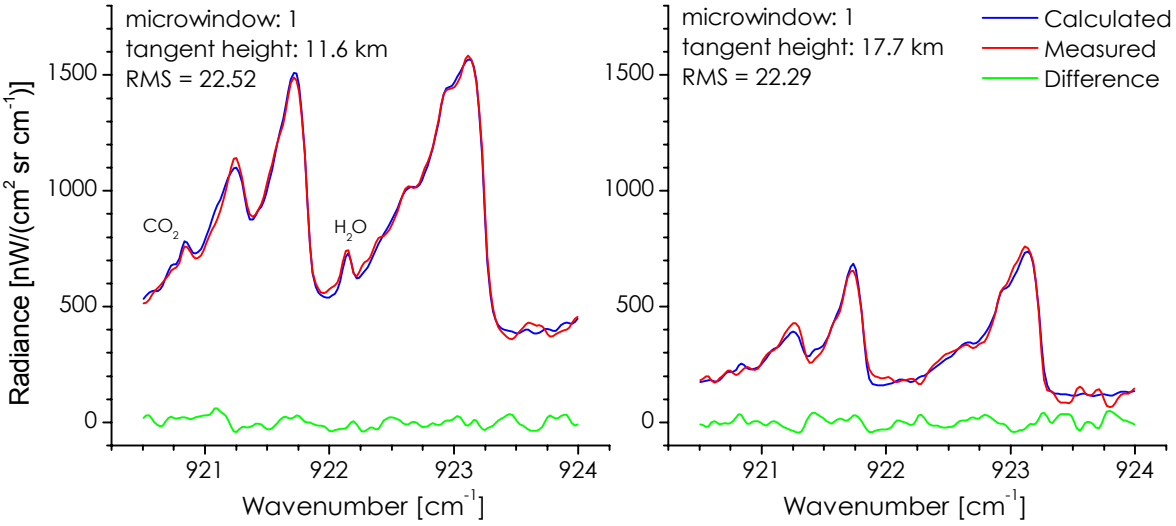

Figure 3.7.1: Sample spectral data for CFC-12 offset retrieval from geometry tangent heights of 11.6 km and 17.7 km

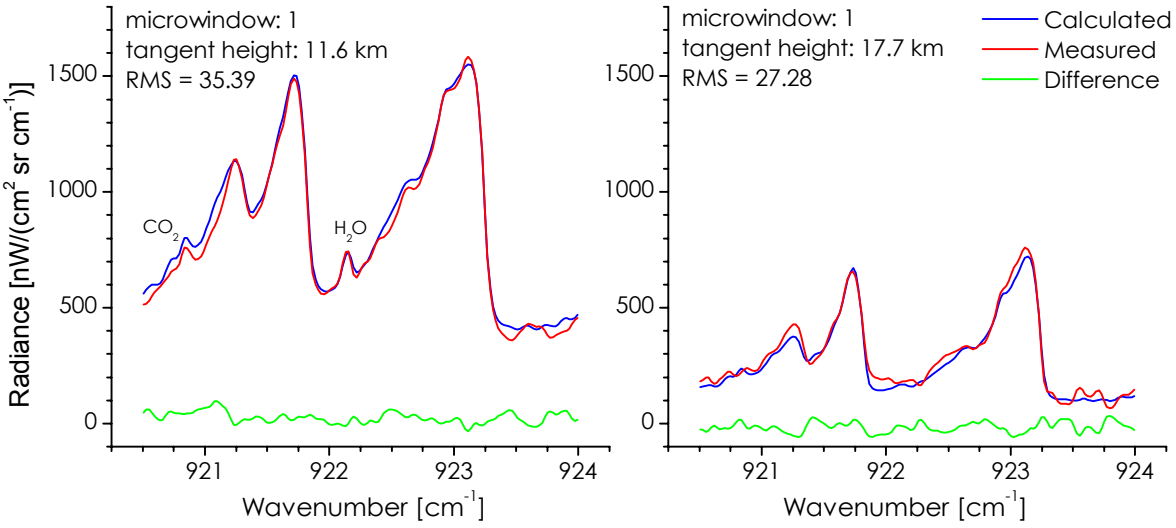

Figure 3.7.2: Sample spectral data for CFC-12 continuum retrieval from geometry tangent heights of 11.6 km and 17.7 km

A sample of the spectra used in the offset retrieval is shown in Figure 3.7.1. The same sample used for the continuum retrieval is shown in Figure 3.7.2. Small CO_2 and H_2O signatures can be seen. The former spectra have better RMS values, but they did not necessarily give better results. Below 14 km, the offset calculations had a tendency to go towards lower concentrations, creating a minimum which shouldn't exist. It was thought that this could be due to aerosol absorption (as suggested for CFC-11 as well), which is why the second calculation with a continuum fit was tried. This did in fact seem to correct the problem to some extent, but the profiles were much less stable. These profile oscillations are linked to the larger RMS values that can be seen in the sample spectra, which indicate that the algorithm has more trouble simulating aerosols. In both calculation series, very strong regularisation had to be used to smooth out the profiles.

3.7.2 Results and Observations

Retrieved CFC-12 VMR profiles from region 1 are shown in Figure 3.7.3. Above the flight level, and down to about 15 km, the offset and continuum retrievals are practically equal, suggesting that this part of the profiles is real. Problems begin, however, beneath the 15 km level. The minimum in the offset retrieval mentioned earlier can be seen here at 13 km. at 10 km, this profile then rises back up to concentrations above the initial guess. This is probably false, since gas VMR should be more or less constant within the troposphere.

The continuum retrieval shows its potential here, as it seems to follow the initial guess in a better manner. However, the retrieval strongly oscillates about the initial guess, and this effect could unfortunately not be eliminated through stronger regularisation. This is probably due to the difficulty in properly simulating aerosol absorption.

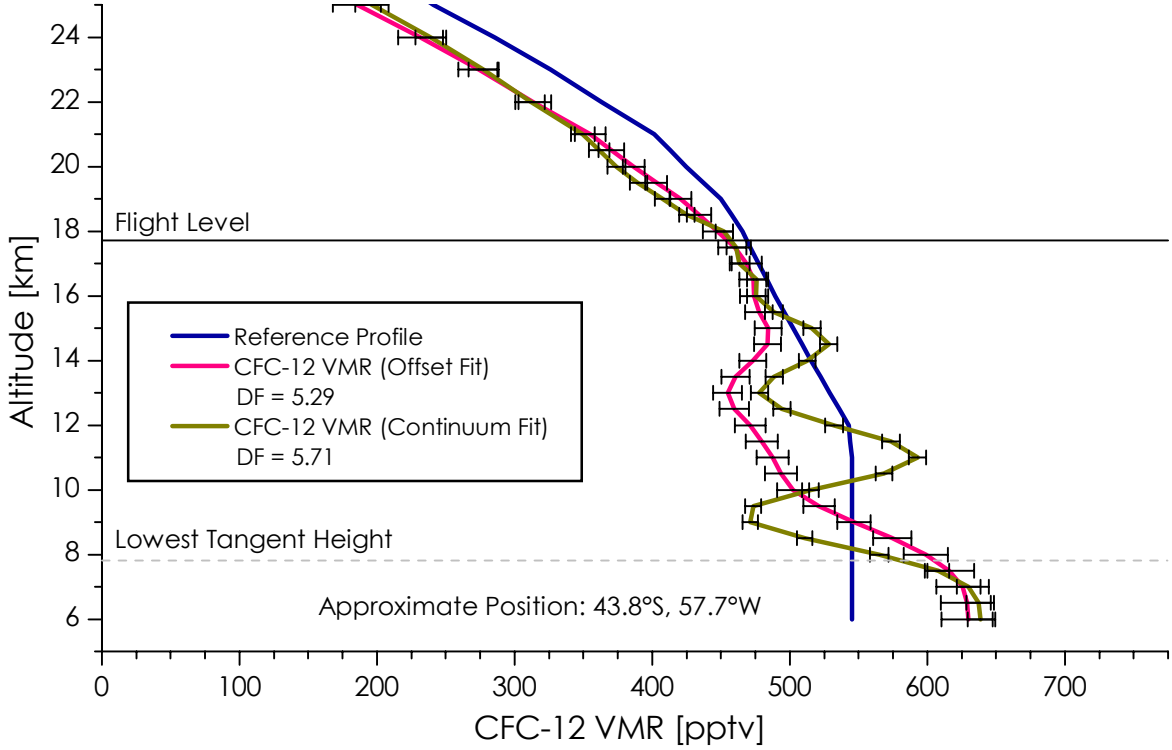

Figure 3.7.3: Retrieved CFC-12 profiles from region 1 with NESR error for offset fit and initial guess

Similar comments can be made for the example retrieval profiles of region 6 in Figure 3.7.4, although the offset retrieval does not swing back to higher concentrations at altitudes below 10 km. This is simply because there are no scan geometries below this level, and hence no information is available. Therefore, the profile simply goes constant. The comparisons to the standard equatorial profile here are not especially good, but the rise of the tropopause does show through comparisons with retrievals from region 1.

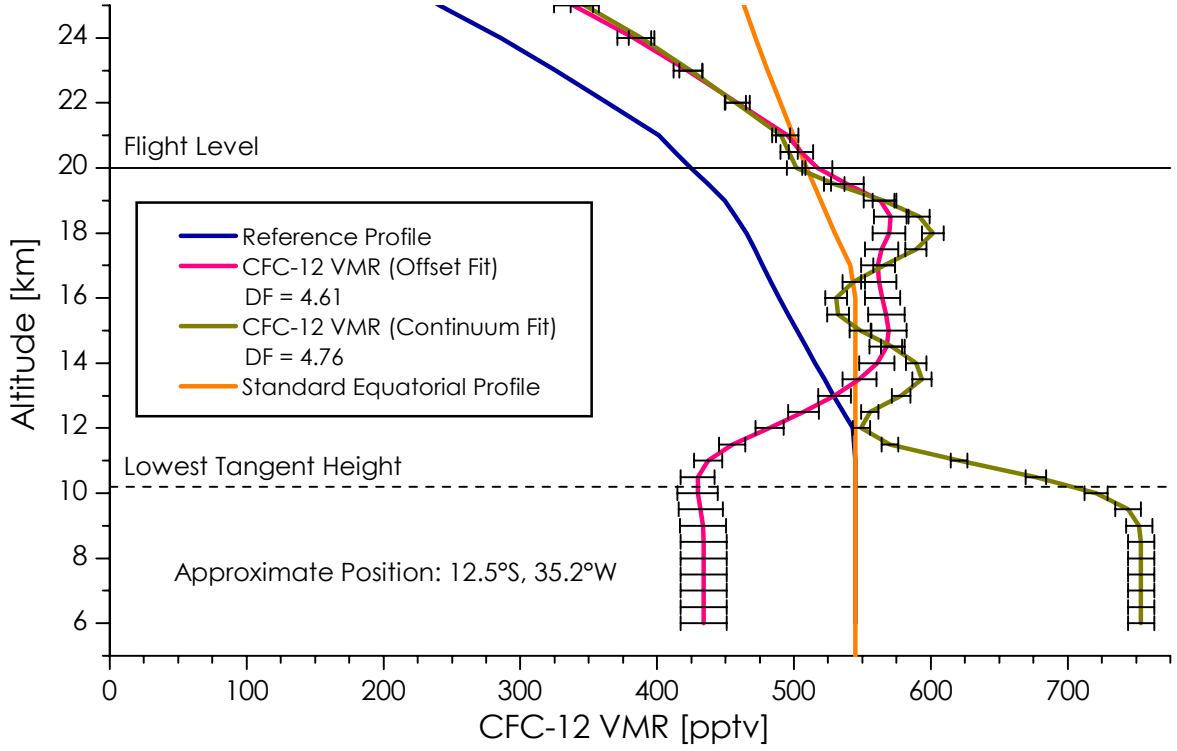

Figure 3.7.4: Retrieved CFC-12 profiles from region 6 with NESR error for offset fit, initial guess, and standard equatorial profile (not used for the retrieval)

Figure 3.7.5 and Figure 3.7.6 respectively show the retrieved two-dimensional distribution of CFC-12 VMR using the offset fit, and using the continuum fit. In both cases, the limit and rise of the troposphere are visible. Above 15 – 16 km, both plots are similar and are therefore probably close to reality. Below this point, however, concentrations within the troposphere seem more coherent in the continuum fit, although lower altitudes contain unlikely high concentrations. These have been plotted as white. All this being said, these retrievals are not so bad considering that they are known to be difficult for this gas. As for previously discussed retrievals, it should be remembered that all information below the lowest tangent heights in regions 4 and 5 should be ignored.

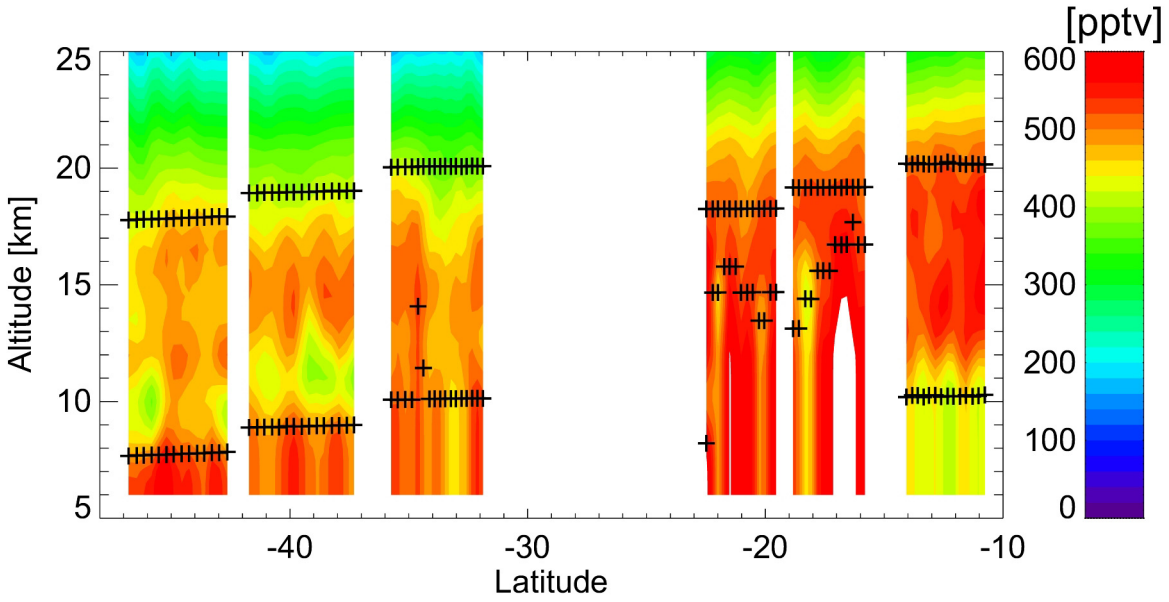

Figure 3.7.5: Two-dimensional distribution of retrieved CFC-12 VMR with offset fit

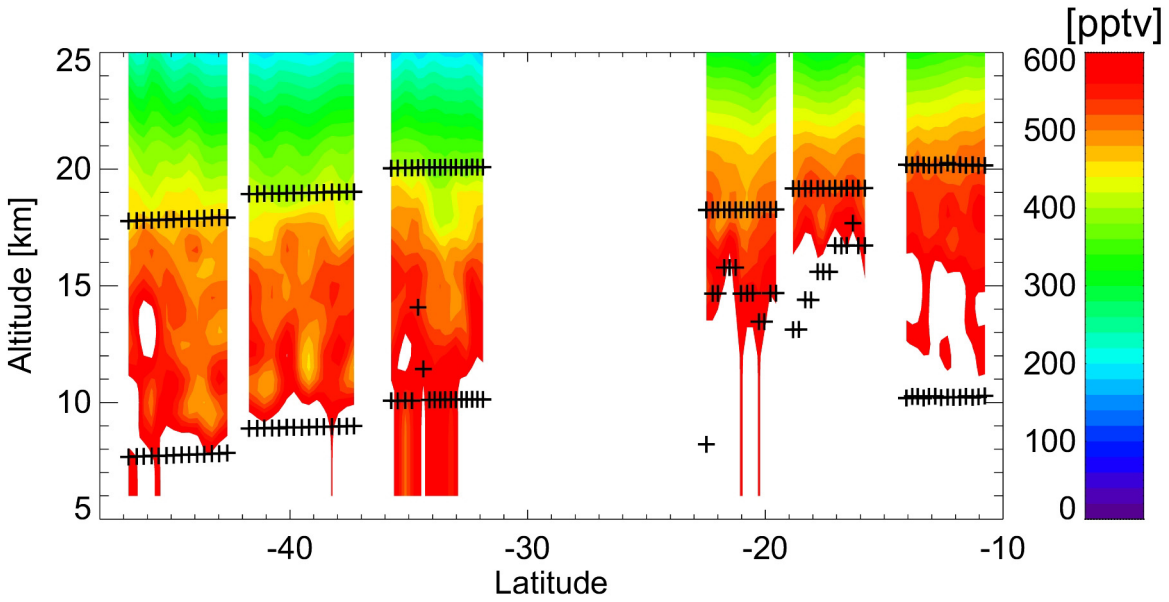

Figure 3.7.6: Two-dimensional distribution of retrieved CFC-12 VMR with continuum fit

3.8 Water Vapour (H_20)

3.8.1 Calculation Procedures

Water vapour was retrieved using 7 microwindows spread out in the range 808 – 948.5 cm^{-1}. The microwindows used were kept very small, in an attempt to eliminate other spectral signatures. As a result, no other gases had to be included in the retrieval, and H_2O was the only fitted parameter which needed to be regularised. Since microwindows 4 and 5 were in spectral ranges also used for CFC-11, phosgene was included here in the forward model radiative transfer calculations for similar reasons (cf. section 3.6.1). Calculation difficulties related to the initial guess profiles brought the need to change the regularisation method. Instead of a standard H_2O profile shape, a constant profile of 0 was used for this retrieval. Other settings were left as standard. A summary of the retrieval settings used is shown in Table 3.8.1.

Microwindows [cm^{-1}]

1	808.23 – 808.33
2	825.11 – 825.24
3	827.60 – 827.76
4	841.75 – 842.06
5	849.40 – 849.64
6	922.00 – 922.26
7	948.10 – 948.43

Fitted Parameters

H_2O VMR	γ_{H2O} = 0.10 (typical DF = 4.2 – 5.3)
Shift	(no regularisation)
Offset	(no regularisation)

Other Settings

forward model P-T profiles	interpolated from retrieved temperature from 18-10-1999
extra forward model gas	Phosgene ($COCl_2$)
regularisation method	First derivative Tikhonov-Phillips with initial guess of 0
regularisation iterations	5

Table 3.8.1: Retrieval parameters for H_2O

Figure 3.8.1 shows sample spectra which were used for the retrieval of water vapour. Although the regularisation was quite strong, the RMS values remain relatively small. This could be a hint to encouraging retrieval calculations. The drop with height of H_2O VMR is linked to the decrease in line strength seen here.

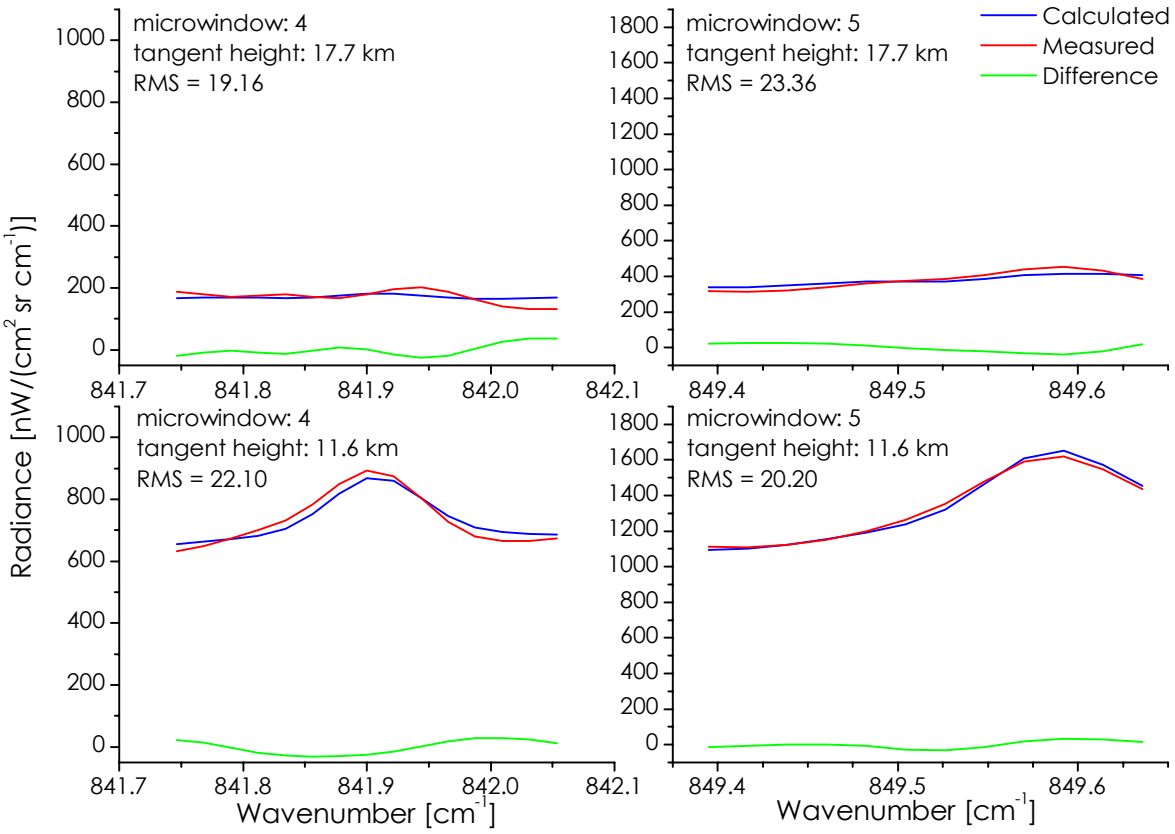

Figure 3.8.1: Sample spectral data for H_2O retrieval from microwindows 4 and 5, and geometry tangent heights of 11.6 km and 17.7 km

As evoked earlier, problems with reference profiles were encountered in the initial test runs for this retrieval. These were related to the concentration gradient at low altitudes. In the middle and lower troposphere, water vapour VMR increases exponentially as altitude decreases. Consequently, a small altitude shift in the standard reference profiles has a strong impact on the shape of the result profiles, because algorithm does the regularisation with respect to the first derivative of the reference profile. This was causing an instability in the results, where a strong overshoot of VMR decrease was creating a profile minimum with negative concentration values. At higher altitudes, where the reference profile had much smaller concentration gradient, the result resumed a realistic shape.

To correct this calculation flaw, standard H_2O profiles were not used for the final calculations. Instead, a simple profile with a constant value of 0 was used. This eliminated the strong dependency on vertical concentration shifts, and so eliminated the negative profile minimum. However, this method in turn created a new problem: in areas where no spectral measurements were present, notably under the lowest tangent height, the result profiles simply followed the initial guess shape, leading to constant concentrations below these levels. Obviously this is not truly the case. This problem, however, is not so important since profile parts where no measurement information is available are always to be ignored.

3.8.2 Results and Observations

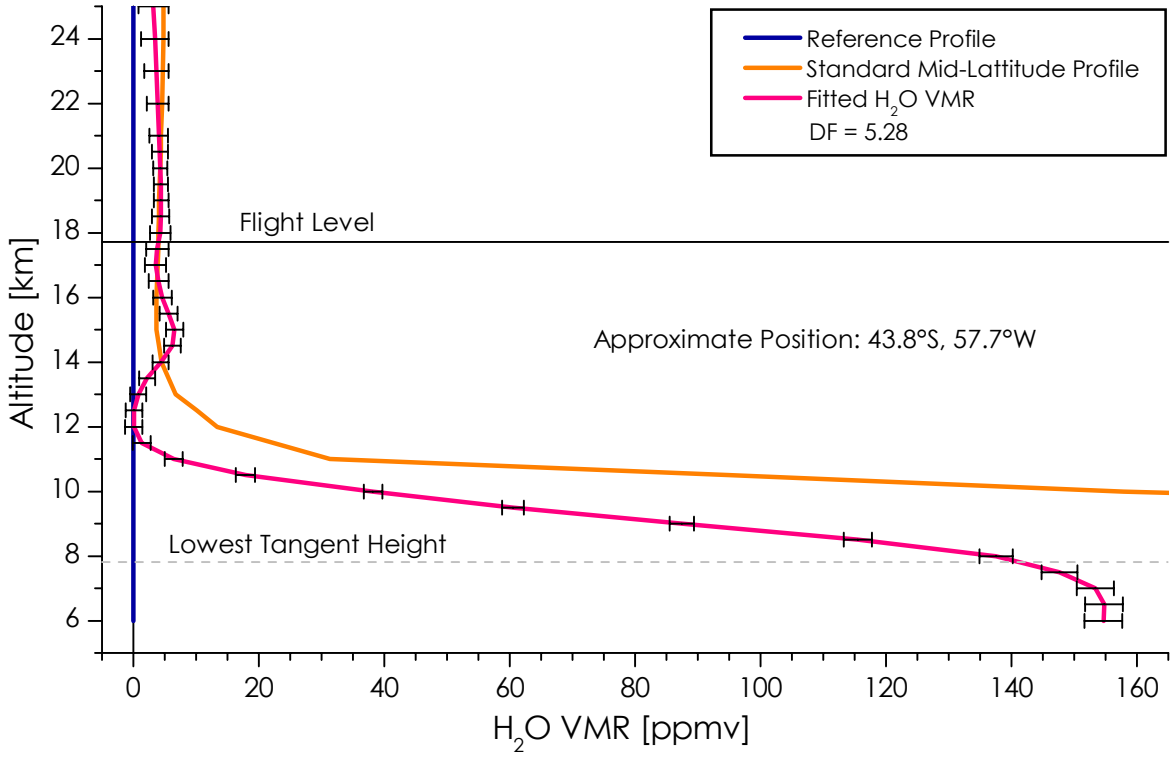

Figure 3.8.2: Retrieved H_2O profile from region 1 with NESR error, initial guess, and standard mid-lattitude profile (not used for the retrieval)

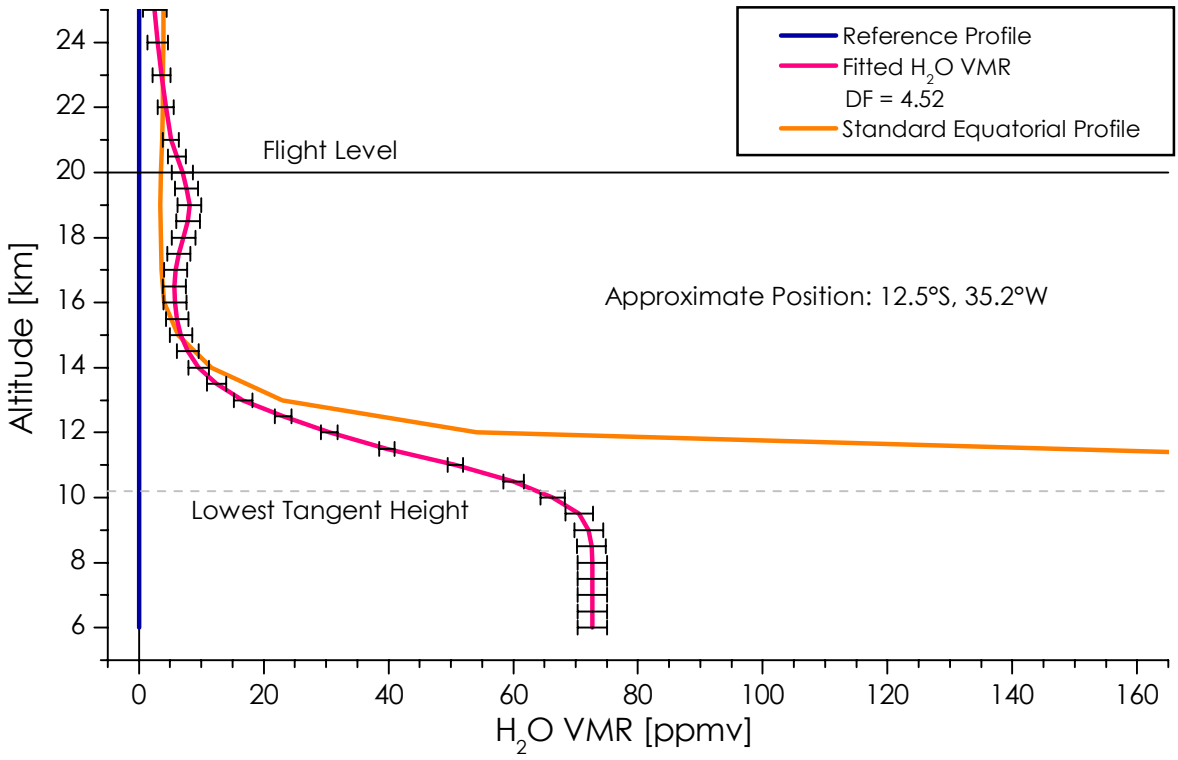

Figure 3.8.3: Retrieved H_2O profile from region 6 with NESR error, initial guess, and standard equatorial profile (not used for the retrieval)

Figure 3.8.2 and Figure 3.8.3 show example retrieval profiles from region 1 and 6 respectively. The standard VMR profile for both latitude regions have been drawn in yellow. These were not used for the calculations, since the constant profile in blue was substituted as the reference profile. The slight altitude shift discussed earlier between the standard profiles and results can clearly be seen here, notably for the profiles from region 1. Comparing the sample profiles from the two regions shows a clear rise in the hygropause between the two latitudes. In region 1, the hygropause is at an altitude of about 11 km, whereas in the tropical latitudes of region 6, it is at about 14 – 15 km.

This rise is also visible when the two dimensional distribution is observed in Figure 3.8.4. Interesting to point out in this result distribution are the small scale gradient changes. Although, globally, the hygropause rises as the equator is approached, this is not done constantly, such as demonstrated by the minimum seen in region 2. Hasty conclusions should not be drawn from this single retrieval, but further work here would be worthwhile to find out if these patterns are real. Nevertheless, at first sight these gradient fluctuations could very well be thought to be true, since they are coherently present in several adjacent profiles at once. As a small note, it should yet again be remembered that information under the lowest tangent heights used should be ignored, since it is a mere reproduction of initial guess shape.

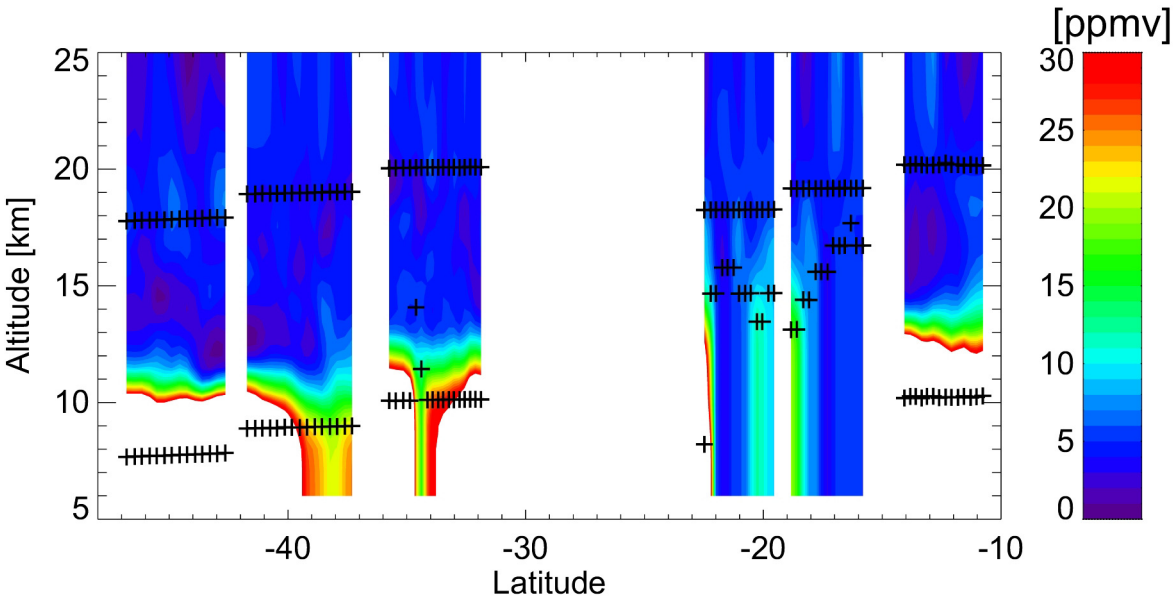

Figure 3.8.4: Two-dimensional distribution of retrieved H_2O VMR

4 Conclusions and Future Work

The primary objective of this work was to analyse MIPAS-STR measurements from 18 October 1999 for a list of atmospheric parameters. All the planned retrievals and more were completed successfully. Problematic retrievals showed areas where the MIPAS-STR experiment needs improvement. The identification of these problems might help for the preparation of the new measurement campaign planed for July 2002. Parts of this report lay foundations for further work.

Temperature, nitric acid and chlorine nitrate were among the retrievals which ran the more smoothly, and which showed numerous signs of being of quite good quality. Comparisons with independent data were possible for the first two. Temperature showed a 4 km rise of the tropopause as the equator is approached, which was also noticed for the various gas retrievals. ECMWF temperatures seemed to be too hot in the tropical tropopause (on average 2.6 K higher than MIPAS-STR results). Nitric acid proved to fit very nicely with the chemical transport model results. The continuum retrieval yielded poor results in terms of absolute values, but was nevertheless successful in detecting upper boundaries of clouds as well as the vertical span of optically thin subvisible cirrus clouds. CFC-11 and 12 showed valuable results, even though the retrievals were troublesome due to aerosols. These two gases – and notably CFC-12 – showed that result profiles of tropospheric gases are highly dependent on how aerosol presence is taken into account in the retrieval. Lastly, water vapour retrievals went fairly well and gave interesting results. The small scale gradient fluctuations observed at low altitudes might be of importance for the further understanding of atmospheric processes. These should be investigated further.

Further work related to the present results should be carried out in several areas. MIPAS-STR was not the only instrument making measurements during the flights, since several in-situ instruments were also gathering information, such as VMRs of O_3, CFC-11, CFC-12, as well as H_2O. Unfortunately this data was not available or readily usable for result comparisons. Therefore, more work is needed to compare the results of the stated gases, once the data becomes available.

Several problems in the retrievals were not fully understood or were difficult to correct. Temperature showed to be on average 3.1 K hotter than in-situ values at flight-level. Preliminary data comparisons for ozone showed similar deviations at this altitude. This is assumed to be of instrumental nature and caused by light scattering from particles on the pointing mirror. Other retrievals yielded problematic results due to other factors. Instrumental noise due to vibrations, unstable calibration functions, and difficulties in simulating aerosols are further examples. Study in these areas would help improve the instrument performance and retrieval algorithms, thus yielding better results for future retrievals.

One last area where more work may be accomplished is the retrieval of other atmospheric parameters for the data from the two discussed flights. The four MIPAS-STR spectral channels contain spectral lines from a number of other gases, some of which are perfectly usable for retrievals. Figure 4.1 shows example spectral signatures from channel 1, which could be used to retrieve other gas VMRs. These were obtained by averaging the measurements from region 6 to minimise noise. CFC-22, SF_6, C_2H_2 and C_2H_6 are among the candidates for which other retrieval calculations could be made.

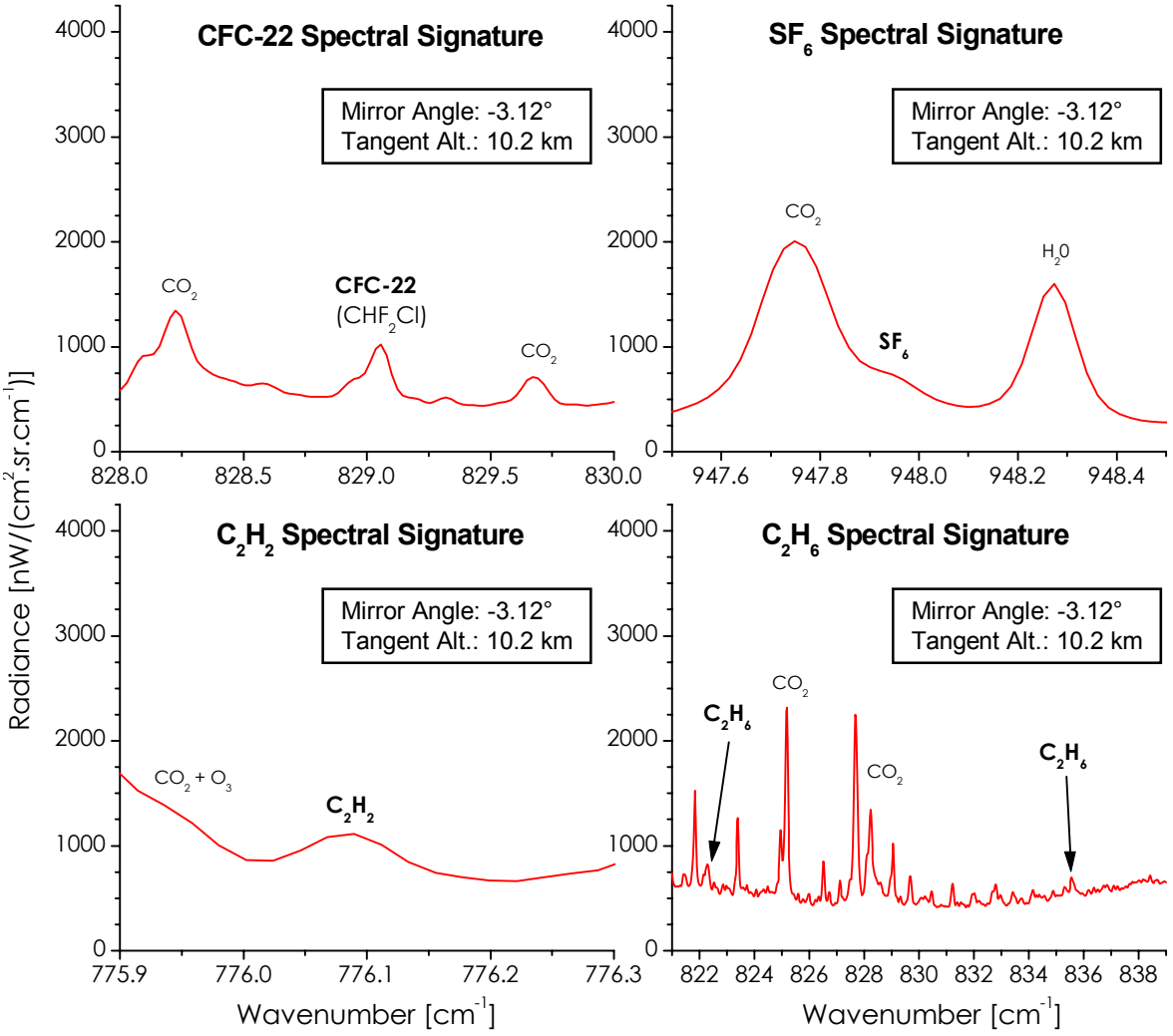

Figure 4.1: Spectral signatures of other species that could be retrieved, obtained by averaging channel 1 data from region 6

References

v. Clarmann T, Dudhia A, Echle G, Flaud JM, Harrold C, Kerridge B, Koutoulaki K, Linden A, Lòpez-Puertas M, Martín-Torres FJ, Reburn J, Remedios J, Rodgers CD, Siddans R, Wells RJ and Zaragoza G. 1998. Study on the simulation of atmospheric infrared spectra. Technical report, European Space Agency, Final Report of ESA Contract12054/96/NL/CN.

Echle G, Oelhaf H, Wegner A. 1992. Measurements of Atmospheric Parameters with MIPAS. European Space Agency, Final Report of ESA Contract 9597/91/NL/SF.

Fischer H. 1992. Remote sensing of atmospheric trace constituents using Fourier transform spectrometry. Berichte der Bunsen-Gesellschaft für physikalische Chemie, Vol. 96, Nr. 3, VCH Verlagsgesellschaft mbH, Weinheim. p 306–314.

Höpfner M. 2002. Private talk.

Höpfner M, Blom CE, v. Clarmann T, Fischer H, Glatthor N, Gulde T, Hase F, Keim C, Kimmig W, Lessenich K, Piesch C, Sartorius C, Stiller GP. 2001. MIPAS-STR data analysis of APE-GAIA measurements. IRS 2000: Current Problems in Atmospheric Radiation, Proceedings of International Radiation Symposium 2000, St. Petersburg, Russia, 24-29 July 2000. William L. Smith and Yuriy M. Timofeyev, Editors. A. Deepak Publishing, Hampton, Virginia. p 1136-1139.

Höpfner M, Blom CE, Echle G, Glatthor N, Hase F, Stiller GP. 2001. Retrieval simulations for MIPAS-STR measurements. IRS 2000: Current Problems in Atmospheric Radiation, Proceedings of International Radiation Symposium 2000, St. Petersburg, Russia, 24-29 July 2000. William L. Smith and Yuriy M. Timofeyev, Editors. A. Deepak Publishing, Hampton, Virginia. p 1121-1124.

Höpfner M, v. Clarmann T, Echle G, Funke B, Glatthor N, Hase F, Kemnitzer H, Kuntz M, Stiller GP, Zorn Z. 1998. The Karlsruhe Optimized and Precise Radiative Transfer Algorithm, Part II: Interface to retrieval applications. SPIE Proceedings, Vol. 3501. p 186-195.

Höpfner M, v. Clarmann T, Fischer H, Friedl-Vallon F, Glatthor N, Kleinert A, Lengel A, Maucher G, Nordmeyer H, Oelhaf H, Stiller GP, Wetzel G. 2002. Evidence of scattering of tropospheric radiation by PSCs in mid-IR limb emission spectra: MIPAS-B observations and KOPRA simulations. Geophys. Res. Lett., Vol. 29, No. 8, 10.1029/2001GL014443.

Keim C. 2002. Entwicklung und Verifikation der Sichtlinienstabilisierung für MIPAS auf dem hochfliegenden Forschungsflugzeug M55 Geophysica.

Dissertation im Fach Physik, IMK, Universität Karlsruhe und Forschungszentrum Karlsruhe.

Phillips D. 1962. A technique for the numerical solution of certain integral equations of the first kind. J. Ass. Comput. Math., 9. p 84-97.

Piesch C, Blom CE, Fischer H, Friedl-Vallon F, Gulde T, Sartorius C, Seefelder M, Wölfel M. 1996. Design of a MIPAS instrument for high-altitude aircraft. Proceedings of the 2nd international airborne remote sensing conference and exhibition, ERIM, Ann Arbor, MI, Vol II. p 199-208.

Stiller GP (Editor), contributions from v. Clarmann T, Dudhia A, Echle G, Funke B, Glatthor N, Hase F, Höpfner M, Kellmann S, Kemnitzer H, Kuntz M, Linden A, Linder M, Stiller GP, Zorn S. 2000. The Karlsruhe Optimized and Precise Radiative transfer Algorithm (KOPRA). Forschungszentrum Karlsruhe, Wissenschaftliche Berichte des Forschungszentrums Karlsruhe FZKA 6487.

Stiller GP, Höpfner M, v. Clarmann T, Echle G, Fischer F, Funke B, Glatthor N, Hase F, Kemnitzer H, Kuntz M, Zorn S. 1998. The Karlsruhe Optimized and Precise Radiative Transfer Algorithm, Part I: Requirements, justification and model error estimation. SPIE Proceedings, Vol. 3501. p 257-268.

Tikhonov A. 1963. On the solution of incorrectly stated problems and a method of regularisation. Dokl. Acad. Nauk SSSR, Vol. 151. p 501.

Acknowledgements

I would first like to thank Prof. Herbert Fischer and PD Dr. Cornelis Blom for the opportunity to carry out a project within the Atmospheric Trace Constituents and Remote Sensing research group. I address my very special thanks to Dr. Michael Höphner who took me under his wing all along the project. He explained everything to me from beginning to end, and was always immediately available to help with retrieval problems.

I would also like to thank Dr. Corneli Keim for all her support. More generally, thanks to all the people in the MIPAS-STR and MIPAS-B research groups who answered any questions I had.

I would lastly like to thank all those who made it possible to use the networking and calculation facilities to carry out my project. This includes especially Claudia Roesner who was very helpful with software and network problems, but also people from the AME group for access to the DEC supercomputer mainframe.

Appendix A: Abbreviations

APE-GAIA:	Airborne Polar Experiment – Geophysica Aircraft In Antarctica
DF:	Degrees of Freedom
ECMWF:	European Centre for Medium-range Weather Forecasts
FOV:	Field Of View
FTIR:	Fourier Transform InfraRed - Spectrometer
FWHM:	Full Width at Half Maximum
GPS:	Global Positioning System
HITRAN:	HIgh-resolution TRANsmission molecular absorption database
IFME:	InterFeroMetric Electronics
ILS:	Instrumental Line Shape
KASIMA:	KArlsruhe SImulation model of the Middle Atmosphere
KOPRA:	Karlsruhe Optimised and Precise Radiative transfer Algorithm
KOPRAFIT:	Algorithm extension from KOPRA
LOS:	Line Of Sight: optical path of the instrument through the atmosphere
LOSE:	Line Of Sight Electronics
MIPAS-B2:	MIPAS for Balloon
MIPAS-FT:	MIPAS - Flugzeug Transall
MIPAS-STR:	Michelson Interferometer for Passive Atmospheric Sounding - STRatospheric aircraft
NESR:	Noise Equivalent Spectral Radiance
NLTE:	Non-Local Thermodynamic Equilibrium
PNRA:	Programma Nazionale di Ricerche in Antartide
RMS:	Root Mean Square
SA:	Selective Availability, service quality restriction used by the US military, no longer active
SNR:	Signal-to-Noise Ratio
UTC:	coordinated universal time, formerly GMT
VMR:	Volume Mixing Ratio

Appendix B: Figures List

Appendix C: Tables List

Appendix D: Additional Reading

Graham Glass, UNIX For Programmers And Users, A Complete Guide, Prentice-Hall International Inc, 1993.

Very clearly presented. The first chapters really focus on the basics, and are written for people who have never even seen a Unix system. Later chapters have incleasingly advanced levels, touching topics useful for the programmer and system administrator. A highly recommended read for new Unix users.

W. Alex und G. Bernör, Einführung in UNIX und C, Universität Karlsruhe, 1991.

Old course manual form the Karlsruhe university. Explains a few useful tricks. Not very well presented, but good for the total newbies. A good read.

John R. Nestor, Joseph M. Newcomer, Paola Giannini, Donald L. Stone, IDL: The Language and Its Implementation, Prentice-Hall International Inc, 1990.

Good read if you're interested in understanding the technicalities of the language. Unfortunately, the style of the book is much too dense and obscure. Confusion and questions is all this book brings. Not enough time is spent to explain the basics of the language. Not a recommended read.

Web Sources:

APE-GAIA homepage:	http://apegaia.iroe.fi.cnr.it
KOPRA documentation:	http://www.imk.fzk.de:8080/-imk2/ame/publications/kopra_docu/
ECMWF database:	http://www.ecmwf.com
HITRAN database:	http://www.hitran.com